Electronic Supplementary Material (ESI) for Journal of Materials Chemistry A.

Organic Cathode Interfacial Materials for Non-Fullerene Organic Solar Cells

Minkyu Kyeong,[a] Jinho Lee,[b,c] Matyas Daboczi,[d] Katherine Stewart,[d] Huifeng Yao,[e] Hyojung Cha,[c] Joel Luke,[d] Kwanghee Lee,[f] James R. Durrant,[c] Ji-Seon Kim,*[d] and Sukwon Hong*[a,f]

[a] Department of Chemistry, Gwangju Institute of Science and Technology, 123 Cheomdan-gwagiro, Buk-gu, Gwangju 61005, Republic of Korea

[b] Department of Physics, Incheon National University, 119 Academy-ro, Yeonsu-gu, Incheon 22012, Republic of Korea.

[c] Department of Chemistry and Centre for Plastic Electronics, Imperial College London, White City Campus, Wood Lane, London W12 0BZ, UK

[d] Department of Physics and Centre for Plastic Electronics, Imperial College London, Exhibition Road, London SW7 2AZ, UK

[e] State Key Laboratory of Polymer Physics and Chemistry, Beijing National Laboratory for Molecular Sciences, Institute of Chemistry, Chinese Academy of Sciences, Beijing 100190, China

[f] Research Institute for Solar and Sustainable Energies, Gwangju Institute of Science and Technology, 123 Cheomdan-gwagiro, Buk-gu, Gwangju 61005, Republic of Korea

*E-mail: ji-seon.kim@imperial.ac.uk (J.K.), shong@gist.ac.kr (S.H.)

1. Materials and analysis methods

All reagents were purchased from commercial sources and were used without any further purification. Materials which were not commercially available were synthesized as following literatures: 2-(5,6-difluoro-3-oxo-2,3-dihydro-1H-inden-1-ylidene)malononitrile (IC-2F),[1] 4-Formyl-*N*,*N*,*N*-trimethyl-benzenaminium iodide,[2] 2,4-(dimethylamino)benzaldehyde,[3] 4-(iodomethyl)benzonitrile,[4] α-iodo-p-tolualdehyde,[5] (4-formylbenzyl)trimethylammonium iodide,[5] α-bromo-p-tolualdehyde,[5] and (4-formylbenzyl)trimethylammonium bromide.[5]

The computational calculations were performed at B3LYP/6-31G(d) level. The molecular structures of the functionalized PEI were simplified to the functionalized *N*-methyl-1-phenylmethanimines without counterions, to reduce the complexity of computation. All of the non-reported compounds were confirmed by NMR (JEOL), MS (LC–MS by Agilent Technologies 6120, FAB–MS by JMS-700 and MALDI-TOF by Voyager DE-STR) and elemental analysis (Elementar). Molecular weight average and polydispersity were measured by GPC (Waters). The polymer solutions were prepared as 10 mg ml^{-1}, and were injected at room temperature under water with $NaNO_3$ as an eluent in flow of N_2 after using polyethylene glycol as standard with different molecular weights. UV–VIS spectroscopy was conducted by Perkin Elmer Lambada 750 in solution and film. For analysis of thin-films, the ionic polymers were spin-coated on ITO glass with and without thermal treatment at 150 °C for 10 min. TGA and DSC were performed by LABSYS EVO (Setaram Instrumentation) in flow of N_2 and by TA instrument Q2 in flow of N_2 at a rate of 10 °C min^{-1} in the temperature range of 20 to 130 °C, respectively. WF values were determined using UPS (ESCALAB 220) and a Kelvin probe instrument (KP6500) with the correspond materials-coated ITO glass by the same method in the previous paper.[6] The atomic concentration of N^+ and N was analyzed by XPS (K-ALPHA$^+$) with the corresponding materials-coated ITO glass. AFM (XE-100 from Park Systems) was performed to confirm the film morphology of the active materials on the corresponding

electrolytes. FT-IR spectra was obtained by Nicolet iS10 (Thermo Scientific) to analyze the vibrational features of the specific chemical bonds using pallets with KBr and the corresponding materials.

2. Mechanistic studies of the reactions

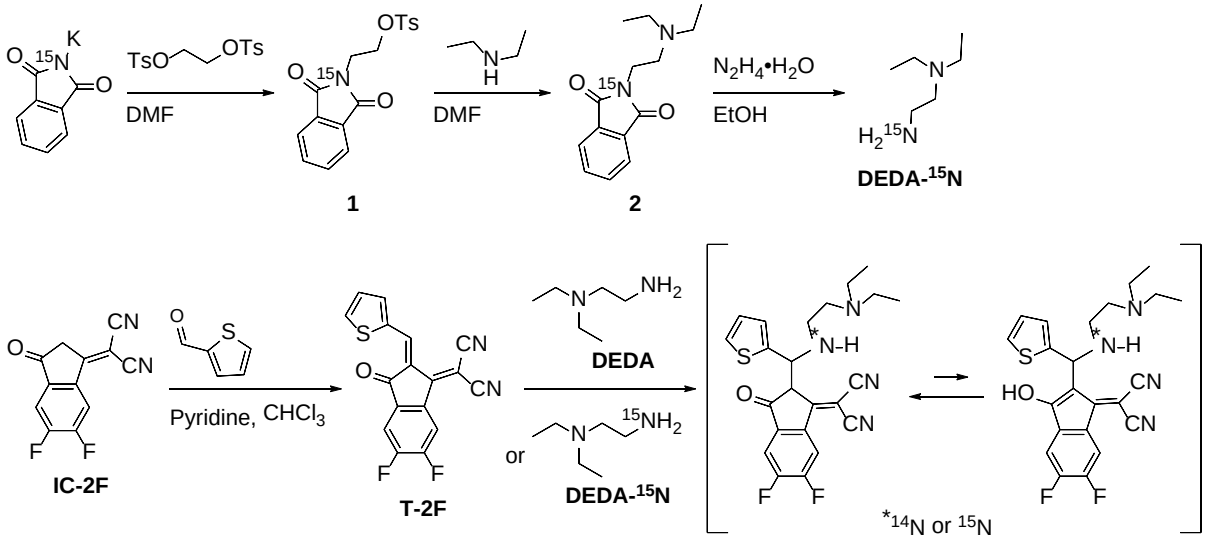

Scheme S1 Synthesis of the model compounds and the reaction.

2-(1,3-dioxoisoindolin-2-yl-^{15}N)ethyl 4-methylbenzenesulfonate (1), 2-(2-(diethylamino)ethyl) isoindoline-1,3-dione-^{15}N (2), N,N-diethylethane-1,2-diamine-^{15}N (DEDA-^{15}N)

The products were prepared following the same procedures in the previous literatures.[7,8] The NMR data showed the same results as those of 2-(1,3-dioxoisoindolin-2-yl)ethyl 4-methylbenzenesulfonate, 2-(2-(diethylamino)ethyl) isoindoline-1,3-dione, DEDA, respectively. ^{15}N NMR (40 MHz, $CDCl_3$, δ (ppm)) was measured as follow: 150.0, 155.6, 17.0, respectively.

2-(5,6-difluoro-3-oxo-2-(thiophen-2-ylmethylene)-2,3-dihydro-1H-inden-1-ylidene)malononitrile (T-2F)

The product was prepared according to the previous literature.[1] Under Ar atmosphere, Thiophene-2-carboxaldehyde (75 mg, 0.67 mmol), 2-(5,6-difluoro-3-oxo-2,3-dihydro-1H-

inden-1-ylidene)malononitrile (IC-2F) (230 mg, 1 mmol), 4 mL chloroform and 129 μL pyridine were used to obtain the orange solid product in 99% yield (215 mg, 0.66 mmol). ^{1}H NMR (400 MHz, $CDCl_3$), δ (ppm): 8.94 (s, 1H), 8.58-8.54 (m, 1H), 8.03 (d, *J* = 5.0, 1H), 7.94 (d, *J* = 3.9, 1H), 7.74-7.71 (m, 1H), 7.30 (dd, *J* = 3.9, 5.0, 1H). ^{13}C NMR ($CDCl_3$, 100 MHz), δ (ppm): 185.5, 158.4, 156.2, 153.6, 144.8, 141.9, 138.6, 137.0, 136.6, 134.9, 128.8, 123.1, 115.2, 113.8, 113.1, 71.8. ESI–MS (m/z): calcd for $C_{17}H_6F_2N_2OS$: 324.0 (M). Found: 325.0 ($M+H^+$).

Preparation of the product between T-2F and DEDA

A solution of T-2F (32 mg, 0.1 mmol) and DEDA (or DEDA-^{15}N) (14 mg, 0.12 mmol) in toluene (1 mL) was heated at 100°C for 1 h under inert atmosphere. After cooling to room temperature, the organic phase was washed by methylene chloride and water. The crude product was purified by a column chromatography to obtain the product. ^{1}H NMR (400 MHz, $CDCl_3$ at RT), δ (ppm): 7.62 (dd, J_{H-F} = 9.5, 6.6, 1H), 7.22 (d, *J* = 5.6, 1H), 7.13 (dd, J_{H-F} = 8.7, 7.3, 1H), 7.09 (dd, *J* = 3.5, 1.5, 1H), 6.91 (dd, *J* = 3.5, 5.1, 1H), 5.70 (s, 1H), 5.29 (s, the tautomer peak), 4.08-3.99 (m, 1H), 3.39-3.31 (m, 1H), 2.63-2.53 (m, 2H), 2.53-2.46 (m, 1H), 2.43-2.29 (m, 3H), 0.95 (t, *J* = 7.2, 6H). ^{13}C NMR ($CDCl_3$, 100 MHz at RT), δ (ppm): 184.7, 160.5, 152.6, 150.6, 150.1, 145.3, 134.8, 132.4, 127.0, 126.3, 125.5, 119.1, 111.4, 111.1, 109.5, 60.7, 60.7, 54.4, 54.2, 47.2, 11.2. ^{1}H NMR (400 MHz, $CDCl_3$ at -50°C), δ (ppm): 11.80 (s, 1H), 7.63-7.56 (m, 1H), 7.24 (d, *J* = 5.0, 1H), 7.15-7.08 (m, 2H), 6.93-6.88 (m, 1H), 5.71 (s, 1H), 5.66 (s, 1H), 4.15-4.02 (m, 1H), 3.40-3.27 (m, 1H), 2.66-2.52 (br, 2H), 2.50-2.41 (m, 1H), 2.40-2.18 (br, 3H), 1.07-0.79 (br, 6H). ^{19}F NMR (380 MHz, $CDCl_3$ at RT), δ (ppm): -133.9, -135.5. ^{15}N NMR (40 MHz, $CDCl_3$ at RT), δ (ppm): 109.2. ^{13}C/DEPT NMR ($CDCl_3$, 100 MHz, 45deg), δ (ppm): 127.0, 126.3, 125.5, 111.4, 111.1, 60.1, 54.3, 47.2, 11.2. ^{13}C/DEPT NMR ($CDCl_3$, 100 MHz, 90deg), δ (ppm): 127.0, 126.3, 125.5, 111.4, 111.1, 60.1, 47.2, 11.2. ^{13}C/DEPT NMR ($CDCl_3$, 100 MHz, 135deg), δ (ppm): 127.0 (+), 126.3 (+), 125.5 (+), 111.4 (+), 111.1 (+), 60.1 (+), 54.5 (-), 54.3 (-), 47.2 (-), 11.2 (+). ESI–MS (m/z): calcd for $C_{23}H_{22}F_2N_4OS$: 440.1 (M). Found:

439.0 ($M–H^+$).

Selection of the appropriate amine for identification of the undesirable reaction

Fig. S1 summarizes our strategy to elucidate the origin of the undesired reaction between the PEI and IT-4F. First, we synthesized T-2F as a model compound for IT-4F; furthermore, appropriate amines (diethylamine as a secondary amine, trimethylamine as a tertiary amine and *N*,*N*-diethylethylenediamine (DEDA) as a primary amine) were chosen as model compounds for PEI (Fig. S1a). To monitor possible reaction products, UV–VIS spectroscopy analysis and Fourier transform infrared (FT-IR) measurement were conducted. As expected, compared with that of the tertiary amine, the secondary and the primary amines were highly reactive to IT-4F. The UV–VIS absorption spectra of the secondary and the primary amines with IT-4F showed the blue-shifted absorptions, whereas the UV–VIS spectrum of the tertiary amine with IT-4F was similar to the spectrum of only IT-4F (Fig. S1b). Furthermore, the absorption spectra of the secondary amine with IT-4F was different from that of the primary amine, indicating the formation of different products. In the FT-IR spectra, a similar tendency was also observed; a nitrile peak appeared at 2193 cm^{-1} for both the PEI/IT-4F and the DEDA/IT-4F mixtures, whereas a nitrile peak appeared at 2208 cm^{-1} for the Et_2NH/IT-4F mixture. In addition, the nitrile peak appeared at the much higher wavenumber than those of the others with a value of 2219 cm^{-1} for the Et_3N/IT-4F mixture and only IT-4F (Fig. S1b). Furthermore, a carbonyl peak appeared at 1697 cm^{-1} for the Et_2NH/IT-4F, whereas the carbonyl peak appeared at 1704 cm^{-1} for the Et_3N/IT-4F mixture and only IT-4F. It is noteworthy that the carbonyl group vibrational peak disappeared in the FT-IR spectra of the PEI/IT-4F and the DEDA/IT-4F mixtures. These UV–VIS and FT-IR spectroscopy results suggest that different products have been generated depending on the type of amine nucleophiles (primary, secondary and tertiary) and that DEDA behaves most similarly to PEI. Therefore, DEDA was selected as the model compound of PEI.

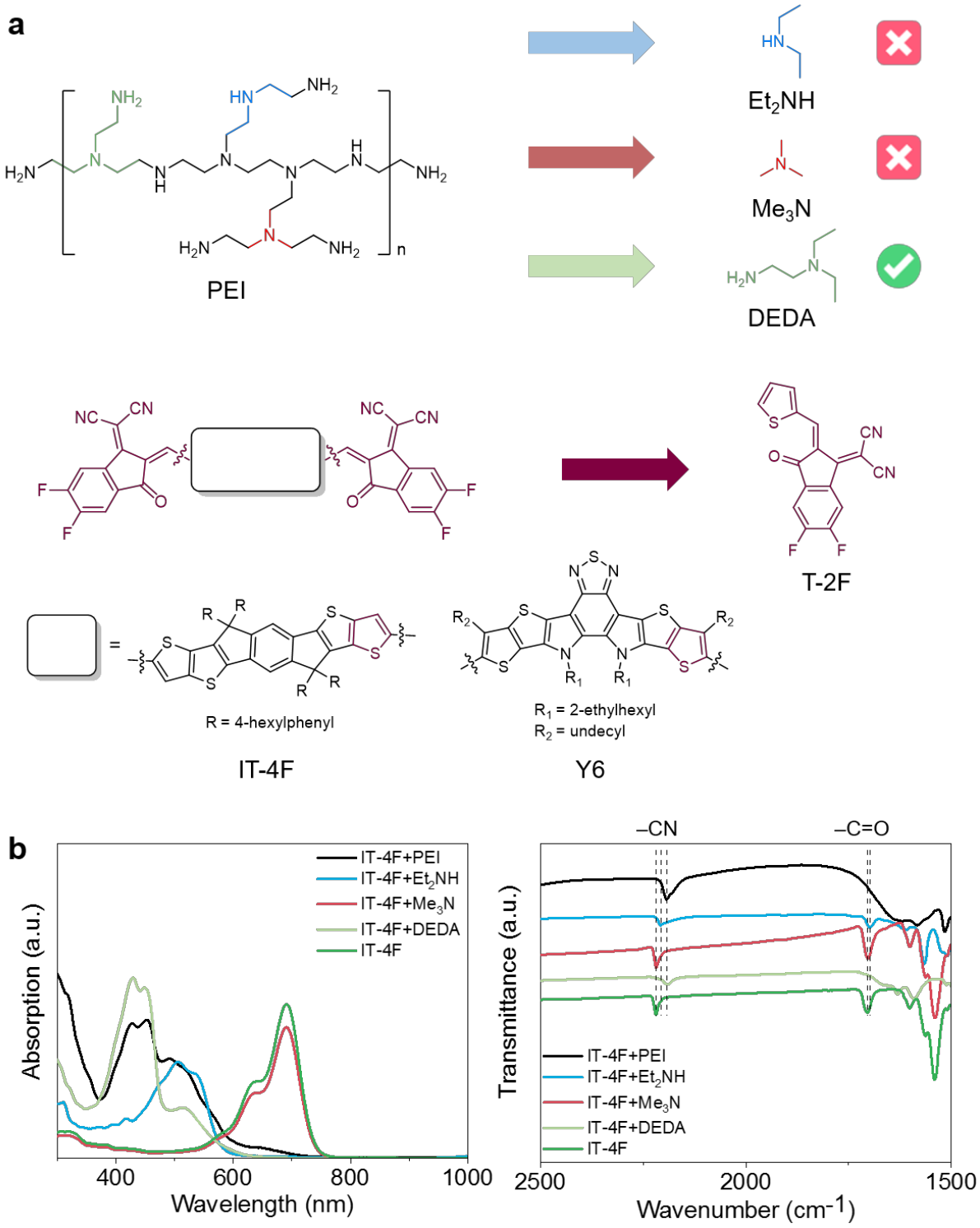

Fig. S1 (a) Model compounds for PEI and the INCN-based NFA. (b) The UV–VIS absorption spectra and FT-IR spectra of IT-4F with and without amines after heat treatment.

3. Synthetic strategy

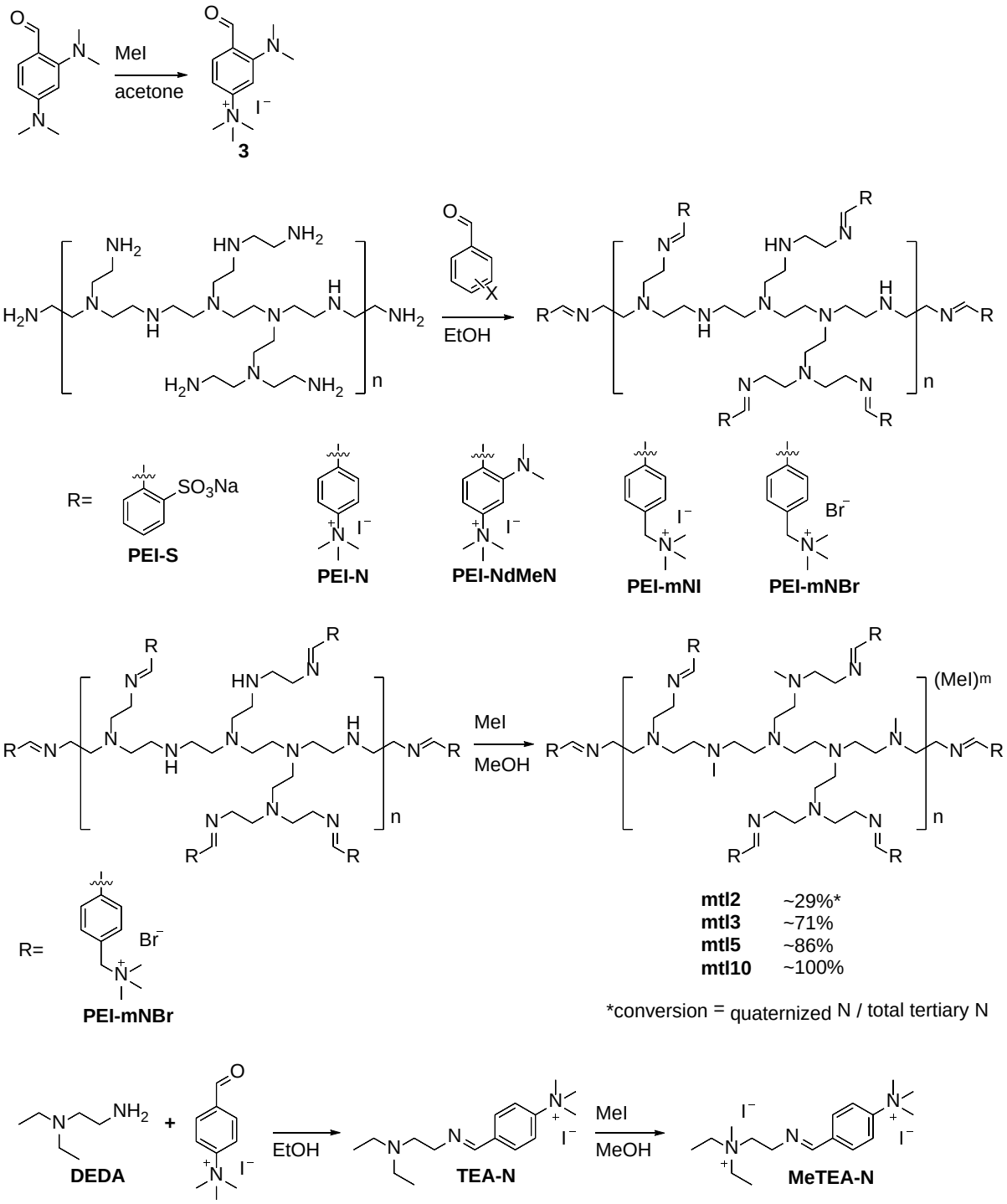

Scheme S2 Overall reaction of the functionalized PEIs and the model compounds for the methylation reaction.

3-(dimethylamino)-4-formyl-N,N,N-trimethylbenzenaminium iodide (3)

To a solution of 2,4-(dimethylamino)benzaldehyde (1.54 g, 8 mmol) in acetone (4 mL) was added methyl iodide (2.99 ml, 48 mmol). The solution was stirred for overnight at 70 °C in a

screw-capped vial. After the precipitate was filtered and washed with acetone, the residual solvent was removed in vacuo to obtain a yellow solid (2.1 g, 6.31 mmol, 79%). ^{1}H NMR (400 MHz, DMSO-d6), δ (ppm): 9.68 (s, 1H), 8.03 (d, *J* = 8.6, 1H), 6.99 (s, d, *J* = 8.6, 2H), 3.72 (s, 9H), 3.19 (s, 6H). ^{13}C NMR (DMSO-d6, 100 MHz), δ (ppm): 189.2, 154.0, 144.0, 114.7, 110.4, 105.2, 55.6, 45.0. FAB–MS (m/z): calcd for $C_{12}H_{19}N_2O^+$: 207.1 (M^+). Found: 207.2 (M^+).

General procedure of synthesis of functionalized PEIs.

A solution of polyethyleneimine (0.05 mmol) and aldehydes (6.25 mmol) in ethanol (3 mL) was heated under reflux for 1.5 d. After cooling to room temperature, the solvent was evaporated, and the mixture was dissolved in water. The solution was purified under dialysis for over 2 days, and the water was removed via freeze-drying process to obtain products. Imine proton peaks in ^{1}H NMR data were only used to determine the successful imine formation reaction.

PEI-S

The product was obtained as a light yellow solid (266 mg, 0.01 mmol, 20%). ^{1}H NMR (400 MHz, DMSO-d6), δ (ppm): 9.21 (s, 1H), 7.93-7.71 (br, 2H), 7.44-7.35 (br, 2H), 3.64 (br, 2H). GPC: Mn 25.7 kDa, Mw 61.8 kDa, *Đ* 2.4. Elemental analysis calcd (%) for $C_{50}H_{67}N_{11}Na_4O_{12}S_4$: C 48.65, H 5.47, N 12.48, S 10.39. Found: C 48.57, H 5.79, N 12.40, S 10.32.

PEI-N

The product was obtained as a dark brown solid (251 mg, $7.5X10^{-3}$ mmol, 15%). ^{1}H NMR (400 MHz, DMSO-d6), δ (ppm): 8.30 (s, 1H), 7.64-7.51 (br, 2H), 6.80-6.67 (br, 2H), 4.13-3.96 (br, 2H), 3.78-3.49 (br, 9H). GPC: Mn 21.1 kDa, Mw 50.0 kDa, *Đ* 2.4. Elemental analysis calcd (%) for $C_{62}H_{103}I_4N_{15}$: C 47.55, H 6.63, N 13.41. Found: C 47.51, H 7.11, N 13.19.

PEI-NdMeN

The product was obtained as a light brown solid (554 mg, 0.015 mmol, 30%). ^{1}H NMR (400 MHz, DMSO-d6), δ (ppm): 8.42 (s, 1H), 7.85 (s, 1H), 7.62-7.52 (br, 2H), 3.63-3.46 (br, 2H), 3.44-2.93 (br, 15H). GPC: Mn 19.9 kDa, Mw 41.0 kDa, *Đ* 2.1. Elemental analysis calcd (%) for $C_{70}H_{123}I_4N_{19}$: C 48.36, H 7.13, N 15.31. Found: C 48.02, H 7.23, N 15.28.

PEI-mNI

The product was obtained as a light yellow solid (618 mg, 0.02 mmol, 40%). ^{1}H NMR (400 MHz, DMSO-d6), δ (ppm): 8.41 (s, 1H), 7.89-7.76 (br, 2H), 7.66-7.57 (br, 2H), 4.58 (br, 2H), 3.74-3.67 (br, 2H), 3.13-3.07 (br, 9H). GPC: Mn 24.4 kDa, Mw 51.3 kDa, *Đ* 2.1. Elemental analysis calcd (%) for $C_{66}H_{111}I_4N_{15}$: C 48.86, H 6.90, N 12.95. Found: C 49.23, H 7.10, N 13.75.

PEI-mNBr

The product was obtained as a light yellow solid (618 mg, 0.02 mmol, 40%). ^{1}H NMR (400 MHz, DMSO-d6), δ (ppm): 8.37 (s, 1H), 7.79-7.68 (br, 2H), 7.57-7.42 (br, 2H), 4.79 (br, 2H), 3.70-3.54 (br, 2H), 3.25-3.14 (br, 9H). GPC: Mn 25.6 kDa, Mw 56.5 kDa, *Đ* 2.2. Elemental analysis calcd (%) for $C_{66}H_{111}Br_4N_{15}$: C 55.27, H 7.80, N 14.65. Found: C 55.63, H 8.59, N 14.97.

General procedure of methylation of PEI-mNBr.

A solution of PEI-mNBr (3.30 X 10^{-3} mmol) and methyl iodide (corresponding equivalents with respect to the secondary amines on the backbone of PEI-mNBr) in methanol (1 mL) was heated at 40 °C for 1 d. After cooling to room temperature, the solvent was evaporated under inert atmosphere, and the mixture was dissolved in water. The solution was purified under dialysis for over 1 day, and the water was removed via freeze-drying process to obtain products (a series of mtl).

mtl2

2 equivalents of methyl iodide were added. The product was obtained as a yellow solid. GPC: Mn 28.9 kDa, Mw 63.6 kDa, *Đ* 2.2. Elemental analysis calcd (%) for $C_{71}H_{123}Br_4I_2N_{15}$: C 48.45, H 7.04, N 11.94. Found: C 48.24, H 6.84, N 11.74.

mtl3

3 equivalents of methyl iodide were added. The product was obtained as a yellow solid. GPC: Mn 28.3 kDa, Mw 57.8 kDa, *Đ* 2.0. Elemental analysis calcd (%) for $C_{74}H_{132}Br_4I_5N_{15}$: C 40.66, H 6.09, N 9.61. Found: C 40.69, H 5.88, N 9.51.

mtl5

5 equivalents of methyl iodide were added. The product was obtained as a yellow solid. GPC: Mn 27.9 kDa, Mw 61.5 kDa, *Đ* 2.2. Elemental analysis calcd (%) for $C_{75}H_{135}Br_4I_6N_{15}$: C 38.69, H 5.85, N 9.02. Found: C 38.34, H 5.99, N 8.81.

mtl10

10 equivalents of methyl iodide were added. The product was obtained as a yellow solid. GPC: Mn 32.2 kDa, Mw 80.6 kDa, *Đ* 2.5. Elemental analysis calcd (%) for $C_{76}H_{138}Br_4I_7N_{15}$: C 36.96, H 5.63, N 8.51. Found: C 36.80, H 5.56, N 8.32.

4-(((2-(diethylamino)ethyl)imino)methyl)-N,N,N-trimethylbenzenaminium iodide (TEA-N)

A solution of N,N-diethylethylenediamine (58 mg, 0.5 mmol) and 4-Formyl-*N*,*N*,*N*-trimethyl-benzenaminium iodide (146 mg, 0.5 mmol) in ethanol (5 mL) was heated at 60 °C for 4 h. After cooling to room temperature, the solvent was removed under inert atmosphere and the precipitate was purified with diethyl ether to obtain a light yellow solid (186 mg, 0.48 mmol,

96%). ^{1}H NMR (400 MHz, DMSO-d6), δ (ppm): 8.40 (s, 1H), 8.09-7.97 (br, 2H), 7.94-7.81 (br, 2H), 3.67-3.56 (br, 11H), 2.65-2.53 (br, 2H), 2.48-2.36 (br, 4H), 0.91-0.79 (br, 6H). ^{13}C NMR (DMSO-d6, 100 MHz), δ (ppm): 160.1, 148.9, 138.0, 129.4, 121.6, 59.6, 57.0, 53.4, 47.4, 12.6. FAB–MS (m/z): calcd for $C_{16}H_{28}N_3^+$: 262.2 (M^+). Found: 262.3 (M^+).

4-(((2-(diethyl(methyl)ammonio)ethyl)imino)methyl)-N,N,N-trimethylbenzenaminium diiodide (MeTEA-N)

A solution of TEA-N (78 mg, 0.2 mmol) and methyl iodide (28 mg, 0.2 mmol) in methanol (1 mL) was heated at 40 °C for 2 h. After cooling to room temperature, the solvent was removed under inert atmosphere, the precipitate was purified with diethyl ether to obtain a yellow solid (96 mg, 0.18 mmol, 90%). ^{1}H NMR (400 MHz, DMSO-d6), δ (ppm): 8.63 (s, 1H), 8.11 (d, *J* = 7.7, 2H), 7.97 (d, *J* = 7.4, 2H), 4.08-4.01 (br, 2H), 3.66 (s, 9H), 3.63-3.60 (br, 2H), 3.47-3.39 (br, 4H), 3.06 (s, 3H), 1.29-1.22 (br, 6H). ^{13}C NMR (DMSO-d6, 100 MHz), δ (ppm): 162.9, 149.3, 137.3, 129.8, 121.7, 60.1, 56.9, 53.6, 47.9, 47.4, 8.2. FAB–MS (m/z): calcd for $C_{17}H_{31}IN_3^+$: 404.2 (M^+). Found: 404.2 (M^+).

General procedure of methylation of N,N-Diethyl-N'-methylethylenediamine

The reaction was performed with the same procedure of preparation of MeTEA-N using various equivalents of methyl iodide.

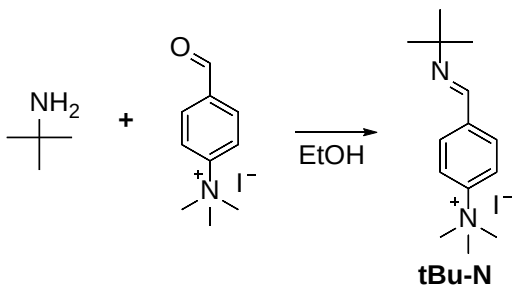

tBu-N

Scheme S3 Synthesis of the model compounds for the chemical stability of the CIMs.

4-((tert-butylimino)methyl)-N,N,N-trimethylbenzenaminium iodide (tBu-N)

A solution of tert-Butylamine (37 mg, 0.50 mmol) and 4-Formyl-*N*,*N*,*N*-trimethyl-benzenaminium iodide (146 mg, 0.50 mmol) in ethanol (5 mL) was heated under reflux for 12 h. After cooling to room temperature, the solvent was removed under inert atmosphere and the precipitate was purified with diethyl ether to obtain a light yellow solid (144 mg, 0.42 mmol, 83%). ^{1}H NMR (400 MHz, DMSO-d6), δ (ppm): 8.43 (s, 1H), 8.06 (d, *J* = 9.1, 2H), 7.97 (d, *J* = 9.2, 2H), 3.65 (s, 9H), 1.24 (s, 9H). ^{13}C NMR (DMSO-d6, 100 MHz), δ (ppm): 153.6, 148.2, 138.1, 128.8, 120.9, 57.5, 56.4, 29.5. FAB–MS (m/z): calcd for $C_{14}H_{23}N_2^+$: 219.2 (M^+). Found: 219.3 (M^+).

4. Materials characterizations

4.1 DFT calculations

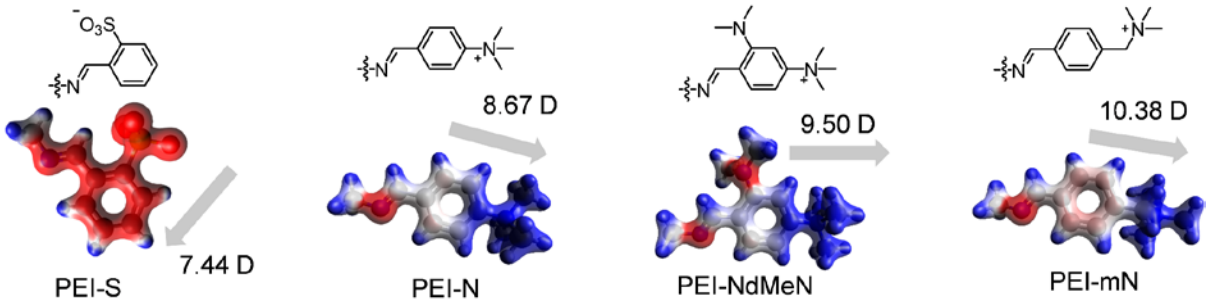

Fig. S2 The electron density distribution with respect to the electrostatic potential and the dipole moment values with the corresponding direction of the functionalized imine groups.

4.2 Thermal, transmittance and work function characterizations

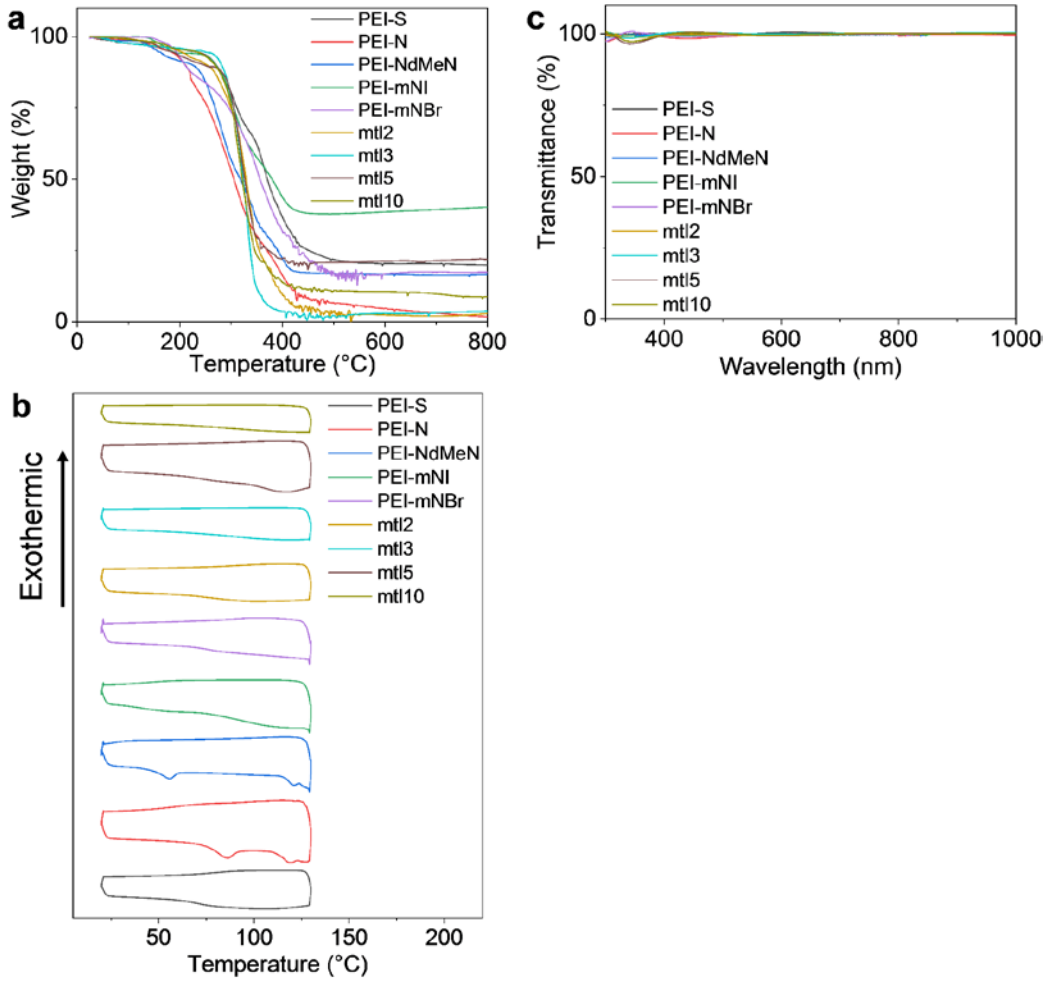

Fig. S3 (a) TGA, (b) DSC and (c) transmittance spectra of the CIMs.

Table S1 Summarized values of the degradation temperature, the glass transition temperature and WF.

CIM	T_d (°C)	T_g (°C)	Work Function (eV)	
PEI-S	220	69	4.12[a]	4.64[b]
PEI-N	179	78	4.03[a]	4.45[b]
PEI-NdMeN	155	50	3.95[a]	4.44[b]
PEI-mNI	184	91	3.87[a]	4.40[b]
PEI-mNBr	192	72	3.81[a]	4.40[b]
mtl2	198	74	4.18[a]	4.69[b]
mtl3	228	78	4.21[a]	4.74[b]
mtl5	177	71	4.26[a]	4.86[b]
mtl10	225	87	4.37[a]	4.89[b]

[a]Values derived from UPS method and [b]values derived from Kelvin probe method.

4.3 XPS characterization

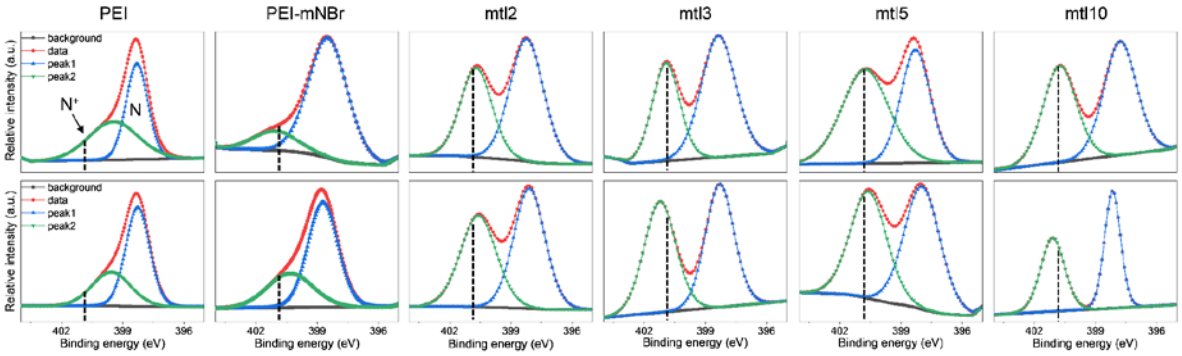

Fig. S4 XPS spectra of the CIMs with and without heat treatment. (*Top: as-cast, bottom: annealed.)

Table S2 The percentage of N^+ out of total nitrogens.

CIM	$[N^+/(N^+ + N)]^a$ (%)	$[N^+/(N^+ + N)]^b$ (%)
PEI	13.7	7.5
PEI-mNBr	18.5	19.6
mtl2	40.8	41.5
mtl3	43.2	43.7
mtl5	46.6	46.7
mtl10	47.7	48.1

[a]As-cast and [b]annealed.

5. Stability examinations of the CIMs

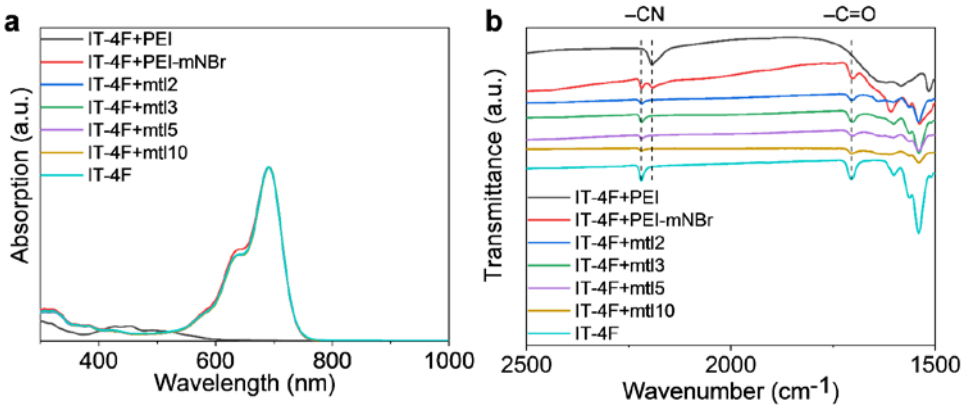

Fig. S5 (a) UV-VIS absorption spectra and (b) FT-IR spectra of IT-4F with and without the CIMs after heat treatment.

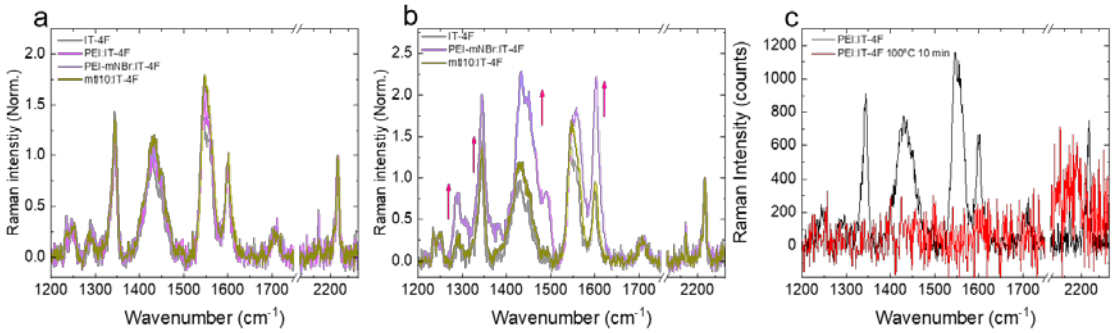

Fig. S6 Representative normalized Raman spectra of the IT-4F and the CIM:IT-4F films under 514 nm laser excitation (a) before and (b) after annealing. (c) Raman spectra of PEI:IT-4F film under 514 nm laser excitation before and after annealing. Under the condition of 100 °C for 10 min, the characteristic Raman peaks of the PEI:IT-4F are completely smeared out.

When the Raman spectra are normalized to the nitrile mode, significant increases in the relative peak intensities of the core group compared to those of the end group are observed: peaks at 1597 and 1344 cm^{-1} for the core phenyl and peaks at 1462 and 1431 cm^{-1} for the thiophenes in the core. The peak at 1544 cm^{-1} associated with the alkenes shows the slight increase and peak broadening, while carbonyl (1700 cm^{-1}) and nitrile (2200 cm^{-1}) peaks are unchanged. The degradation of the products presented above results in disruption of the interunit alkenes, breaking conjugation between the core and end groups, which can concentrate electron density to the core, and thereby leading to an increase in Raman intensity of core vibrational modes as

we observed experimentally.

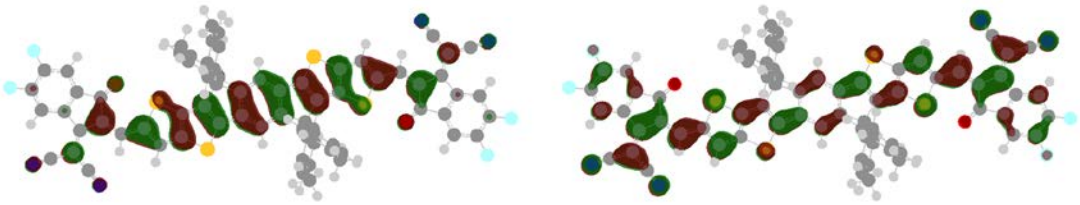

HOMO simulated -5.59 eV LUMO simulated -3.50 eV

Fig. S7 Density functional theory (DFT) simulation for orbital visualization at minimized energy structures.

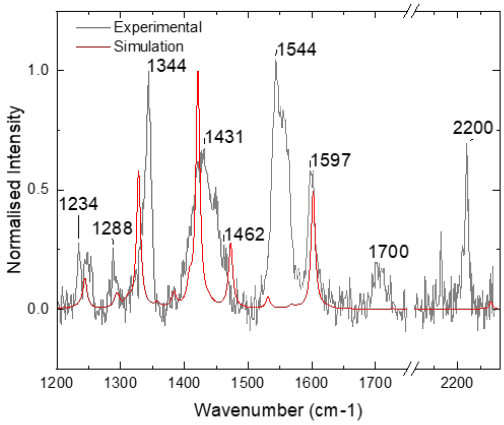

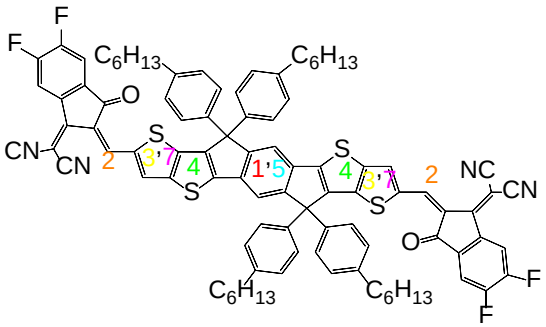

Peak Number	Wavenumber (cm^{-1})	Assignment
	2200	End group nitrile
	1700	End group carbonyl
1	1597	Core central phenyl
2	1544	Alkenes particularly on bridge
3	1462	Core outer thiophenes, C-C
4	1431	Core inter thiophenes, C-C
5	1344	Core central phenyl, symmetric expansion
6	1288	H wagging
7	1234	Core outer thiophene C=C

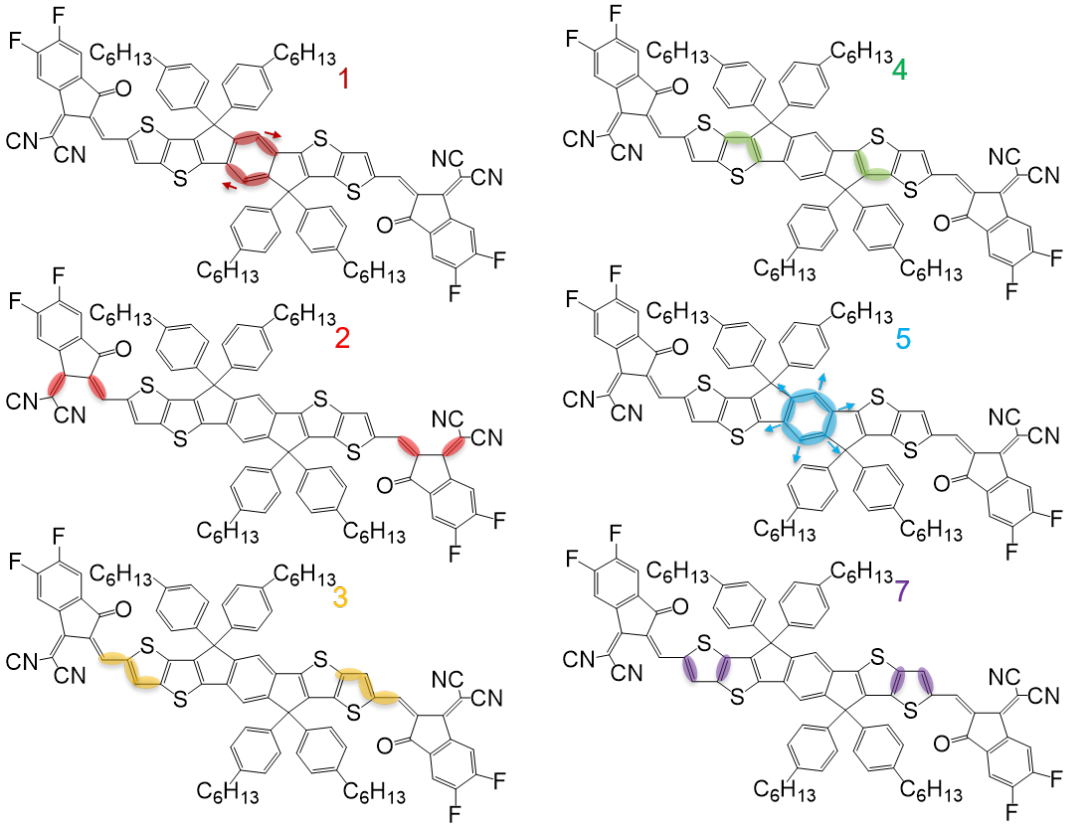

Fig. S8 Simulated and experimental Raman spectra of the IT-4F film obtained by 514 nm excitation. Vibrational Raman peaks assignments of IT-4F, derived from DFT simulation.

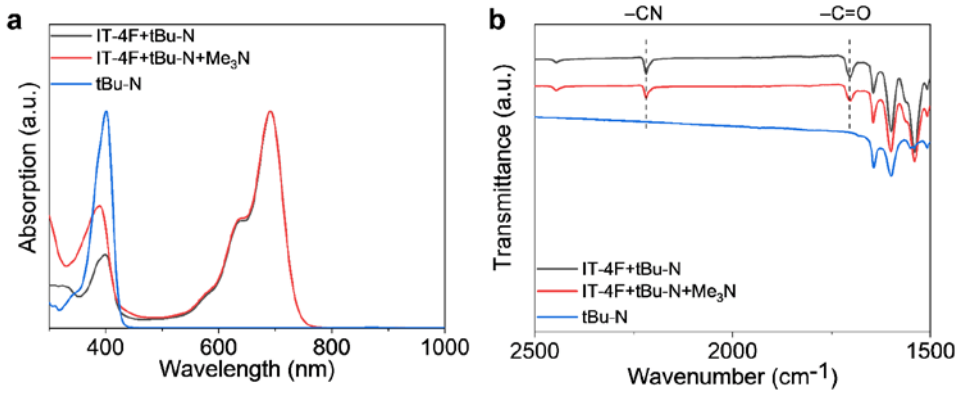

Fig. S9 (a) UV-VIS absorption spectra and (b) FT-IR spectra of only tBu-N and the mixture of IT-4F and tBu-N with and without Me_3N after heat treatment.

6. Solar cell fabrication and characterizations

The PEI and PEI-S were dissolved in isopropanol and dimethylsulfoxide, respectively, to form 0.05% solutions. The other polyelectrolytes including PEI-N, PEI-mNI, PEI-mNBr, mtl2, mtl3, mtl5, and mtl10 were dissolved in 2-methoxyethanol to form 0.05% solutions. All of the solutions were stirred for overnight before use. The ZnO precursor solution was prepared by mixing 220 mg of zinc acetate dihydrate, 60 µl of ethanolamine, and 2 ml of 2-methoxyethanol. The photoactive material solutions were prepared by dissolving PBDB-T-SF:IT-4F (1:1 w/w) and PTB7-Th:$PC_{71}BM$ (1:1.5, w/w) in the chlorobenzene with small amount of 1,8-diiodooctane for 0.5% and 3%, respectively. For a high performance application, PBDB-T-2F:Y6 (1:1.2, w/w) was dissolved in chloroform with small amount of 1-chloronaphthalene for 0.5%.

The glass/ITO substrates were pre-cleaned before the device fabrication in an ultrasonic bath of water with detergent, acetone, and isopropyl alcohol for 20 min each, and then dried at 70 °C oven. The electron transport layers (i.e, ZnO or polyelectrolytes) were spin-coated at 5000 rpm for 30 s onto the ITO after the fully dried ITO-coated glass substrates were treated with UV-ozone for 10 min. For the device with ZnO electron transport layer, ZnO solution was spin-coated at 4000 rpm for 40 s, followed by annealing at 150 °C for 20 min. Subsequently, the photoactive solution was spin-coated at 1000 rpm for 40 s to obtain the desired thickness. In the case of PBDB-T-2F:Y6, the solution was spin-coated at 3000 rpm for 40s. Then the samples were loaded in a vacuum chamber, and at a high vacuum condition of 5×10^{-6} torr, MoO_3 (10 nm) and Ag (100 nm) were sequentially deposited to complete the device fabrication. The actual device area was defined by the overlap area between the top and the bottom electrodes yielding 0.045 cm^2. *J–V* characteristics were measured using a Keithley 2400 source meter under AM 1.5G solar illumination with an irradiation intensity of 100 mW cm^{-2} which was obtained from calibrated Xenon lamp using a silicon reference cell. For accurate measurements, the external quantum efficiency (EQE) spectra were measured using a 100 W tungsten halogen lamp

(Bentham IL1 with Bentham 605 stabilized current power supply) coupled to a monochromator with computer-controlled stepper motor. Incident photon flux on the sample was calibrated using a UV-enhanced silicon photodiode for spectral mismatch correction before measurement. To exclude the effect of second-order diffraction at the wavelengths longer than 580 nm, a 590 nm long-pass glass filter was used. Delay time during the measurement was sufficient to ensure the stabilization of the current. Electrochemical impedance spectroscopy (EIS) was performed using an Autolab potentiostat PGSTAT101 in a frequency range between 0.1 and 1 MHz at 0.8 V and open-circuit condition for dark and light conditions, respectively. A white light LED lamp was used as light source for EIS measurements under illumination.

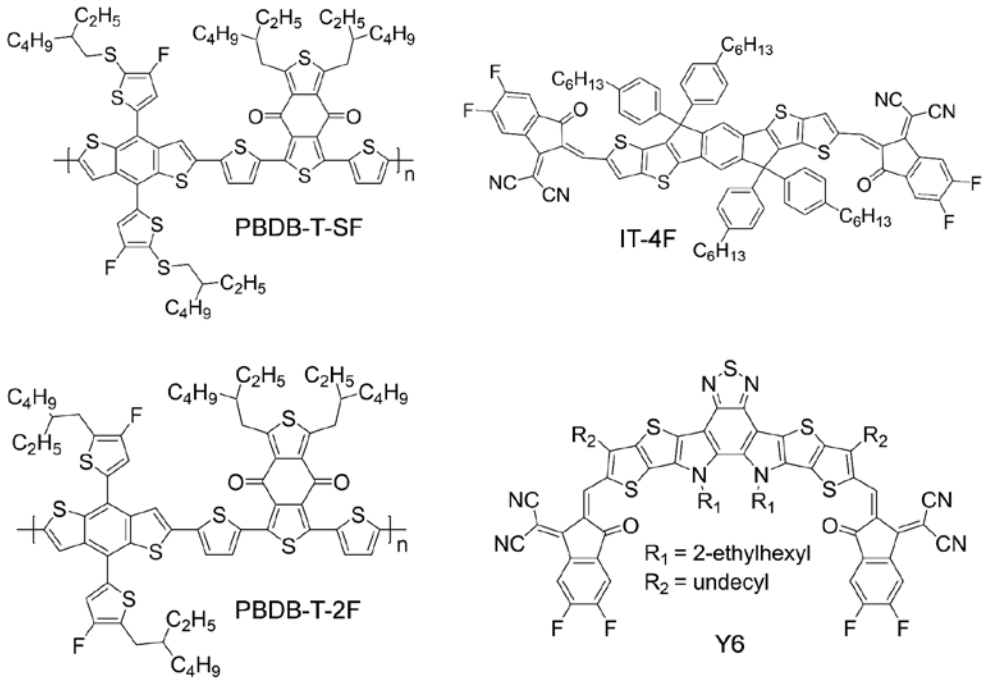

Fig. S10 Molecular structure of the photoactive materials used in this study.

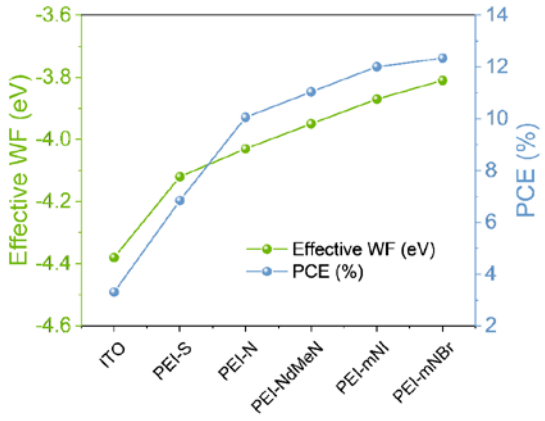

Fig. S11 WF-PCE relationship for the inverted NFSCs.

6.1 Application of the CIMs to the PTB7-Th:$PC_{71}BM$ FSCs

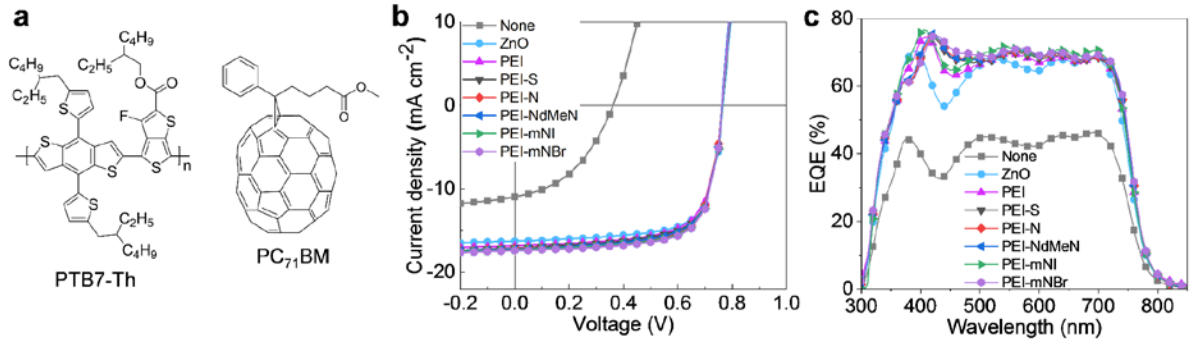

Fig. S12 (a) Molecular structure of the photoactive materials in the FSCs. (b) *J-V* characteristics and c) corresponding EQE spectra of the devices.

Table S3 Photovoltaic parameters of the PTB7-Th:$PC_{71}BM$ OSCs with the various CIMs.

CIM	V_{oc} (V)	J_{sc} (mA cm^{-2})	Calculated J_{sc} (mA cm^{-2})	FF	PCE (%)		R_s [Ω cm^2]	R_{sh} [Ω cm^2]
					Average	Best		
None	0.34 ± 0.02	9.93 ± 1.02	10.38	0.44 ± 0.02	1.14 ± 0.87	2.01	120.8	996
ZnO	0.76 ± 0.01	15.94 ± 0.32	15.83	0.71 ± 0.01	8.80 ± 0.35	9.15	34.6	6799
PEI	0.75 ± 0.01	16.43 ± 0.39	16.47	0.69 ± 0.01	8.69 ± 0.39	9.08	33.1	6313
PEI-S	0.75 ± 0.01	16.57 ± 0.53	16.64	0.68 ± 0.02	8.64 ± 0.49	9.13	32.6	5833
PEI-N	0.75 ± 0.01	16.72 ± 0.45	16.78	0.70 ± 0.01	8.94 ± 0.37	9.31	32.2	6325
PEI-NdMeN	0.75 ± 0.01	16.83 ± 0.38	16.83	0.70 ± 0.01	9.02 ± 0.36	9.38	29.7	6491
PEI-mNI	0.75 ± 0.01	16.90 ± 0.41	16.87	0.71 ± 0.01	9.16 ± 0.41	9.57	31.7	6613
PEI-mNBr	0.75 ± 0.01	16.97 ± 0.43	16.98	0.71 ± 0.01	9.19 ± 0.42	9.61	30.9	6894

6.2 *In-situ* resonant Raman spectroscopy measurements

A Renishaw in Via Raman microscope with InGaAs detector was used to collect both Raman spectra and photoluminescence (PL) with a 50x objective in a backscattering configuration. Both measurements were collected using a 514 nm argon ion laser at 2 mW power (Raman spectra) and 5.5 μW power (PL spectra) and the laser probe was defocused to ~10 μm. Calibration of the filter and grating was performed using the well-defined 520 cm^{-1} peak of a Si reference. The sample was contained in a nitrogen purged Linkam THMS600 sample chamber.

6.3 Application of the CIMs to the PBDB-T-SF:IT-4F NFSCs

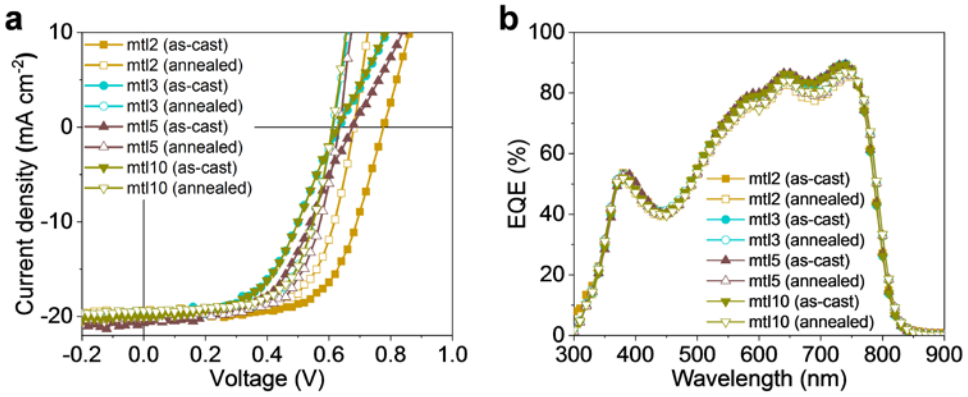

Fig. S13 (a) *J-V* characteristics and (b) corresponding EQE spectra of the devices with the methylated functionalized-PEIs.

Table S4 Photovoltaic parameters of the PBDB-T-SF:IT-4F OSCs with the methylated CIMs.

CIM	Annealing	V_{oc} (V)	J_{sc} (mA cm^{-2})	Calculated J_{sc} (mA cm^{-2})	FF	PCE (%)		R_s [Ω cm^2]	R_{sh} [Ω cm^2]
						Average	Best		
mtl2	as-cast	0.76 ± 0.02	19.40 ± 0.72	19.15	0.61 ± 0.02	9.13 ± 0.77	9.90	85.7	5165
	annealed	0.69 ± 0.01	18.54 ± 0.83	18.52	0.66 ± 0.02	8.85 ± 0.39	9.24	50.7	6804
mtl3	as-cast	0.61 ± 0.02	19.31 ± 1.39	19.03	0.49 ± 0.02	6.02 ± 0.67	6.69	140.8	2386
	annealed	0.62 ± 0.01	19.15 ± 0.64	18.92	0.62 ± 0.02	7.90 ± 0.64	7.76	52.3	3796
mtl5	as-cast	0.66 ± 0.02	19.29 ± 0.76	19.13	0.51 ± 0.02	6.56 ± 0.76	7.32	146.9	1554
	annealed	0.63 ± 0.01	18.41 ± 1.04	18.77	0.63 ± 0.03	8.15 ± 0.93	9.08	40.4	3858
mtl10	as-cast	0.61 ± 0.01	19.42 ± 0.37	19.06	0.51 ± 0.01	6.11 ± 0.24	6.35	137.5	2038
	annealed	0.61 ± 0.01	18.81 ± 0.89	18.76	0.64 ± 0.01	7.81 ± 0.37	8.17	48.1	3379

*Every annealed samples indicate 150 °C for 10 min.

To investigate the charge separation and collection efficiencies, we measured the dependence of photocurrent (J_{ph}) on the effective voltage (V_{eff}) under the light power density of 100 mW cm^{-2} on the surface of the films. The J_{ph} is determined by the current density under illumination after subtraction of the corresponding dark current ($J_{ph} = J_{illumination} - J_{dark}$). The V_{eff} is determined by the voltage at $J_{ph} = 0$ (V_0) after subtraction of applied voltage (V_a) ($V_{eff} = V_0 - V_a$). At high V_{eff}, J_{ph} becomes saturated and saturation current density (J_{sat}) can be used to calculate the maximum charge generation (G_{max}) from the formula $J_{sat} = qLG_{max}$, in which q and L represent the elementary charge and the thickness of the photoactive layer, respectively. The similar G_{max} values indicate that there is no significant difference of overall light harvest between the devices.[9,10] Further, the efficiency of charge carrier transport/collection processes can be estimated by the J_{ph}/J_{sat} values at voltage of maximum power point. The J_{ph}/J_{sat} value of 96.02% for PEI-mNBr based devices is higher than those of other CIMs, reflecting enhanced charge transport/collection along with FFs of the devices.

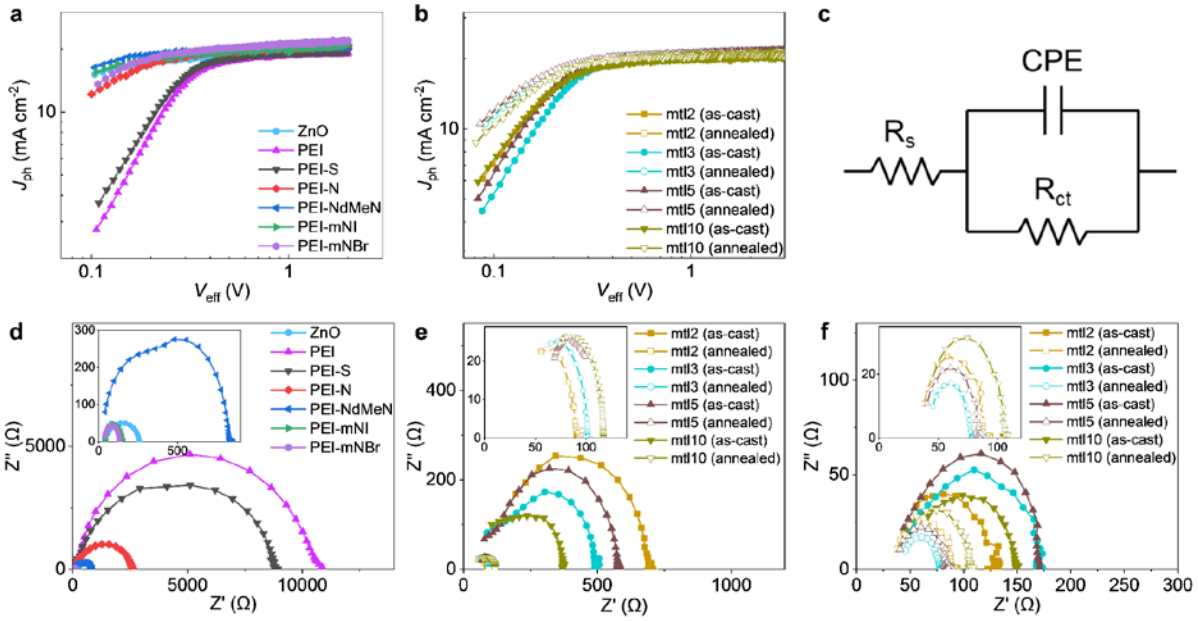

Fig. S14 (a,b) J_{ph}–V_{eff} characteristics for the devices with the CIMs. (c) equivalent circuit of the device to fit the impedance data. Impedance spectra for the devices with the CIMs under (d,e) dark and (f) illumination conditions.

Table S5 The G_{max}, J_{ph}/J_{sat}, R_s, and R_{ct} values calculated from the J_{ph}–V_{eff} and impedance data for the NFSCs with the different CIMs.

CIM	G_{max} (10^{22} cm^{-3} s^{-1})	J_{ph}/J_{sat} (%)	R_s (Ω)		R_{ct} (Ω)	
			dark	light	dark	light
ZnO	1.15	95.94	37	46	219	62
PEI	1.01	92.79	35	44	10828	467
PEI-S	1.07	93.22	46	51	8793	320
PEI-N	1.18	94.68	31	54	2543	94
PEI-NdMeN	1.19	95.21	28	52	812	80
PEI-mNI	1.19	95.77	42	46	111	57
PEI-mNBr	1.25	96.02	37	47	94	52
mtl2	1.20 (1.22)	94.88 (95.25)	188 (54)	54 (37)	505 (37)	76 (54)
mtl3	1.17 (1.21)	94.76 (95.12)	79 (64)	49 (44)	415 (38)	120 (34)
mtl5	1.21 (1.24)	95.05 (95.43)	76 (68)	43 (39)	501 (31)	127 (46)
mtl10	1.16 (1.19)	94.52 (94.97)	101 (73)	66 (43)	269 (44)	84 (64)

*The values in the parenthesis indicate annealed (150 °C for 10 min) samples. All the rest of them are as-cast samples.

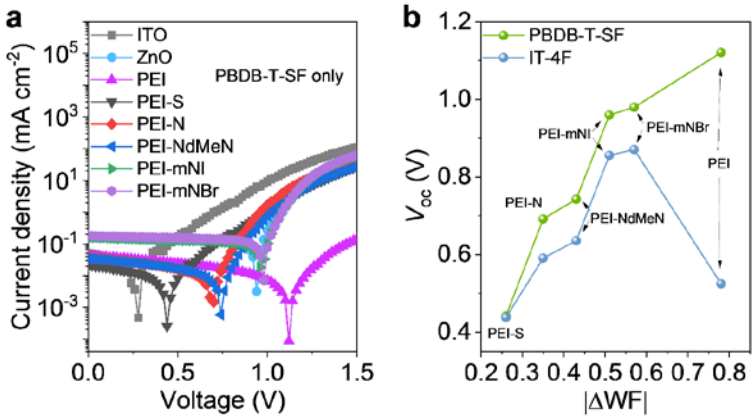

Fig. S15 (a) *J-V* characteristics of the homo-junction device with donor PBDB-T-SF polymer and various CIMs and (b) corresponding V_{oc} values.

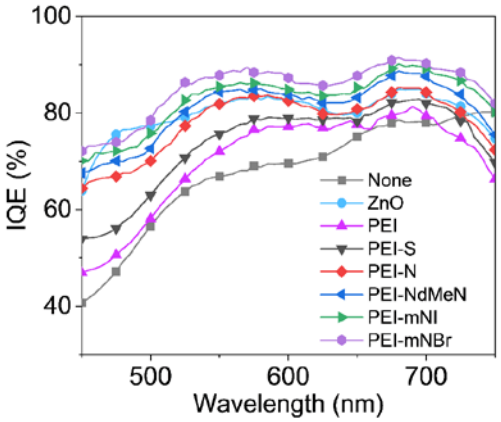

Fig. S16 IQE spectra of the NFSC devices with different CIMs.

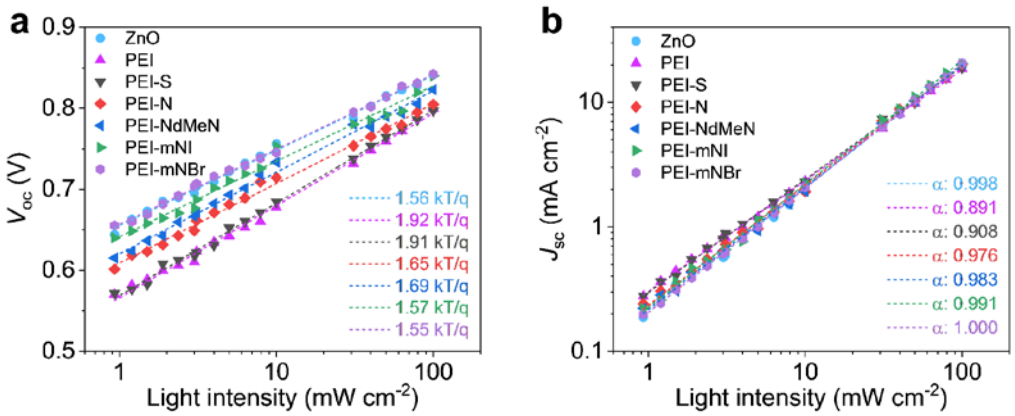

Fig. S17 Dependence of (a) V_{oc} and (b) J_{sc} on light intensity for the OSCs with various CIMs.

6.4 Energy level and surface photovoltage (SPV) measurements

The work function and surface photovoltage measurements were performed using an APS04 (KP Technology). In this system a vibrating tip Kelvin probe (KP) is applied to measure the work function (WF) of the thin layers deposited on a conductive substrate. The samples were grounded during the measurement and the contact potential difference between the tip (2 mm, gold alloy) and the sample was measured in dark until an equilibrium value was reached. The absolute work function of the sample was calculated by adding the equilibrium contact potential difference value to the work function of the tip, which was determined on the same day using a cleaned silver reference. The absolute work function of the silver reference was measured by air photoemission spectroscopy (APS) as part of the calibration process. SPV was recorded by measuring the dark work function of the samples for 20 s then under white light illumination (20 mW/cm^2) for 100 s and finally in dark again for the SPV decay.

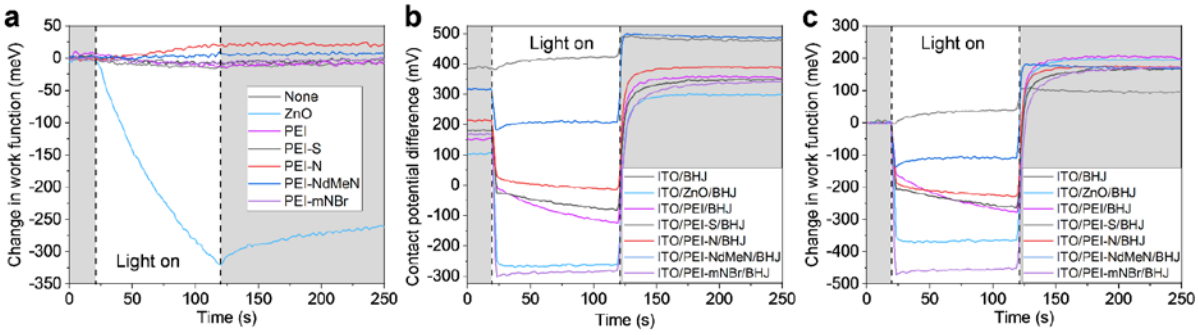

Fig. S18 SPV response for the ITO/CIM and the ITO/CIM/BHJ samples upon illumination. a ITO/CIM, b ITO/CIM/BHJ, and c ITO/CIM/BHJ samples normalized to their dark WF.

6.5 The morphology of the photoactive materials characterization

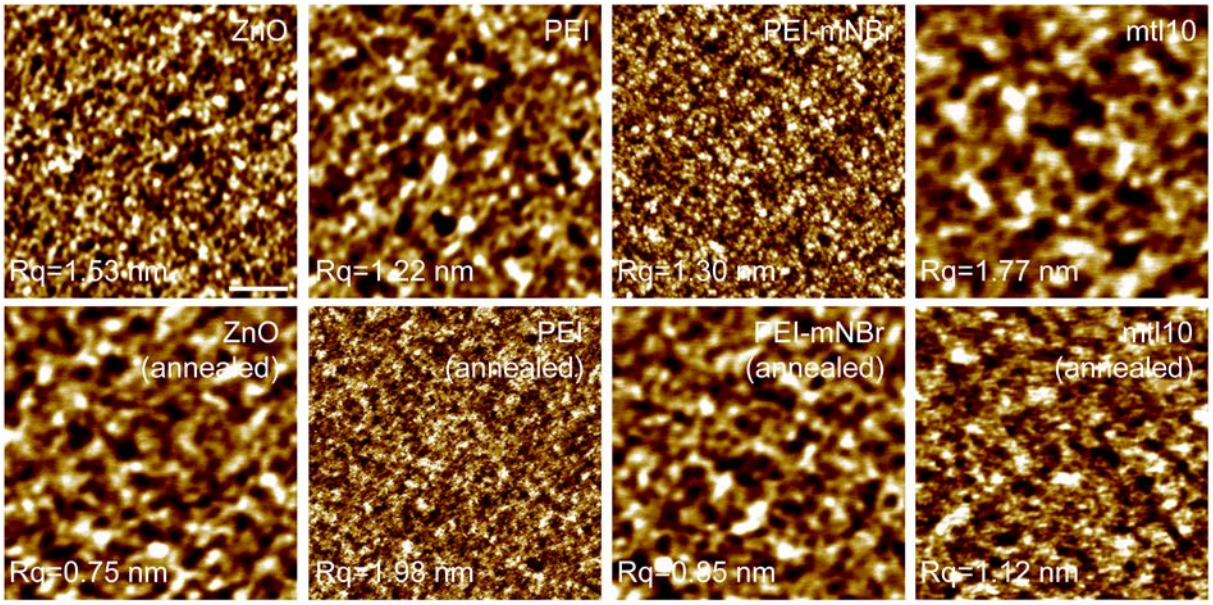

Fig. S19 Atomic force microscopy (AFM) images of pristine and thermally annealed (100 °C) PBDB-T-SF:IT-4F films coated on ZnO, PEI, PEI-mNBr, and mtl10 CIMs. *Scale bar: 2 μm.

7. NMR spectra

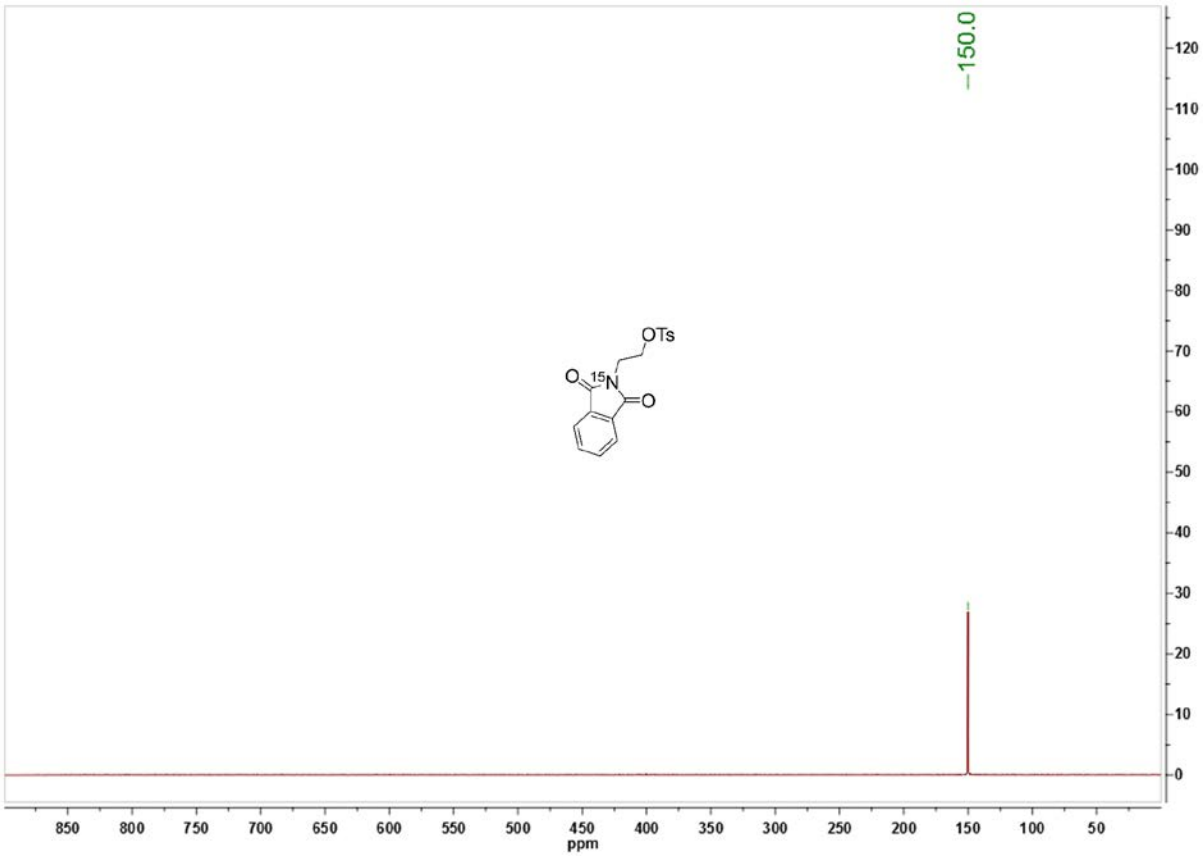

Fig. S20 ^{15}N NMR spectra of 1.

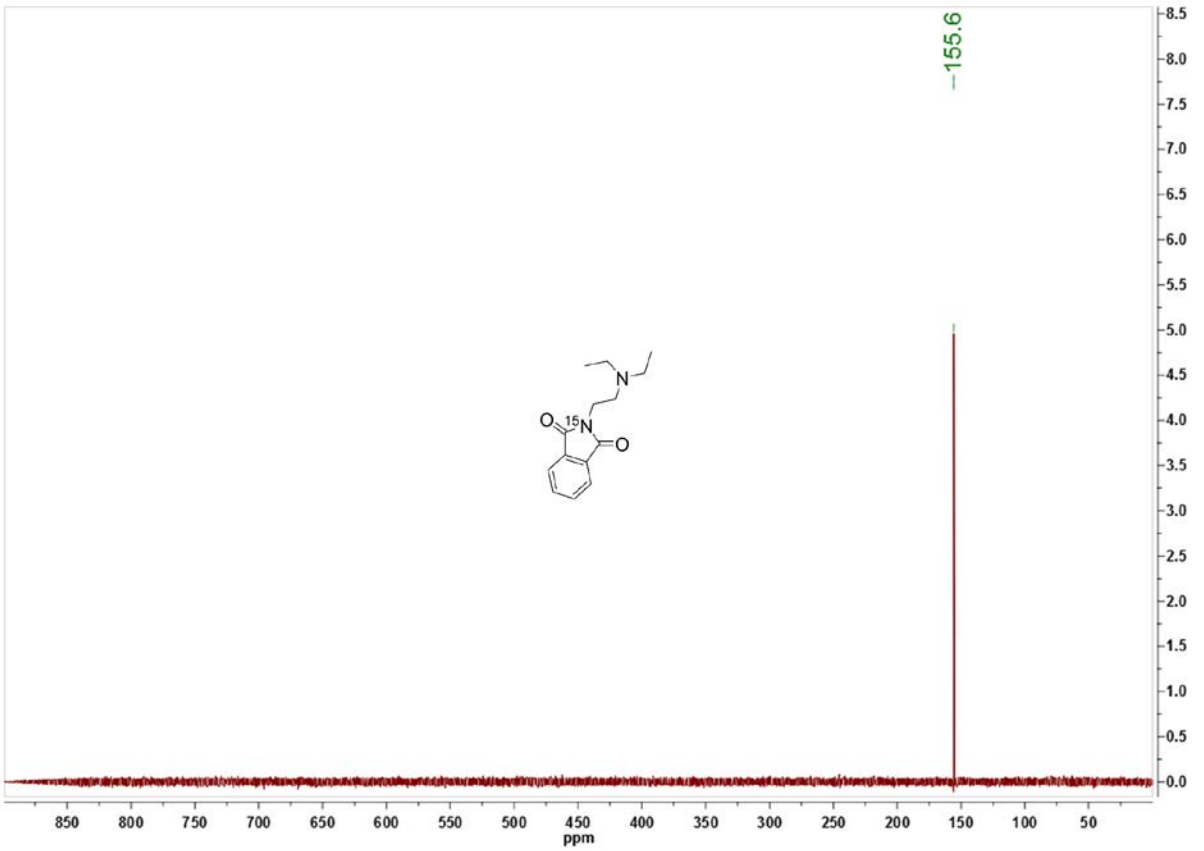

Fig. S21 ^{15}N NMR spectra of 2.

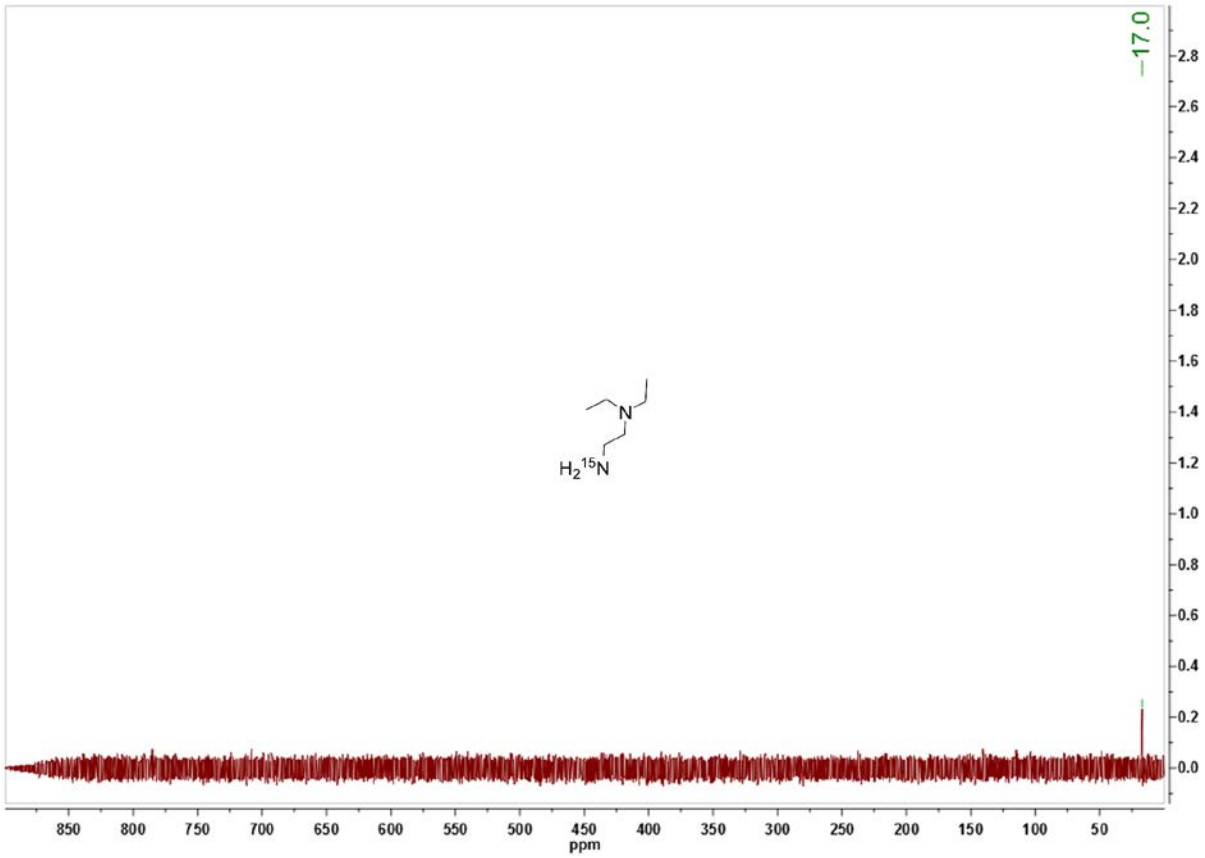

Fig. S22 ^{15}N NMR spectra of DEDA-^{15}N.

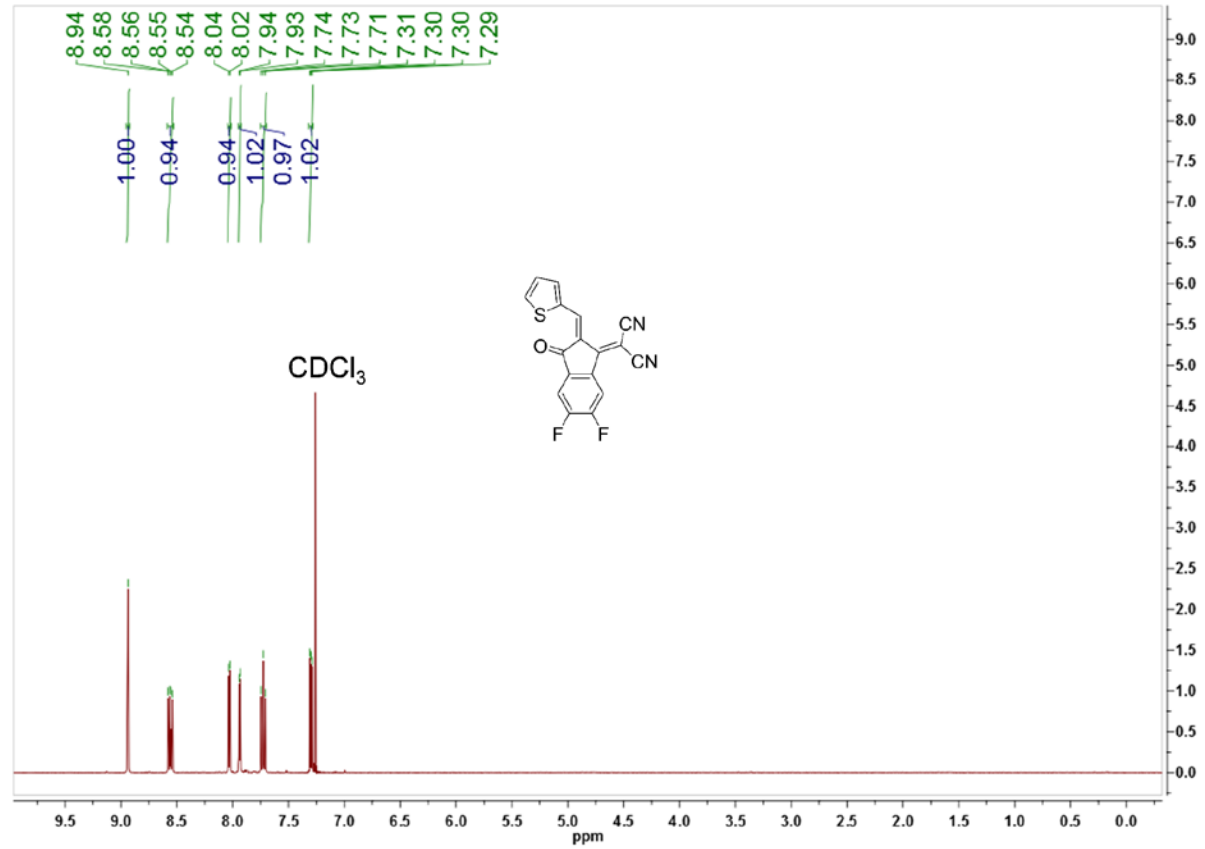

Fig. S13 ^{1}H NMR spectra of T-2F.

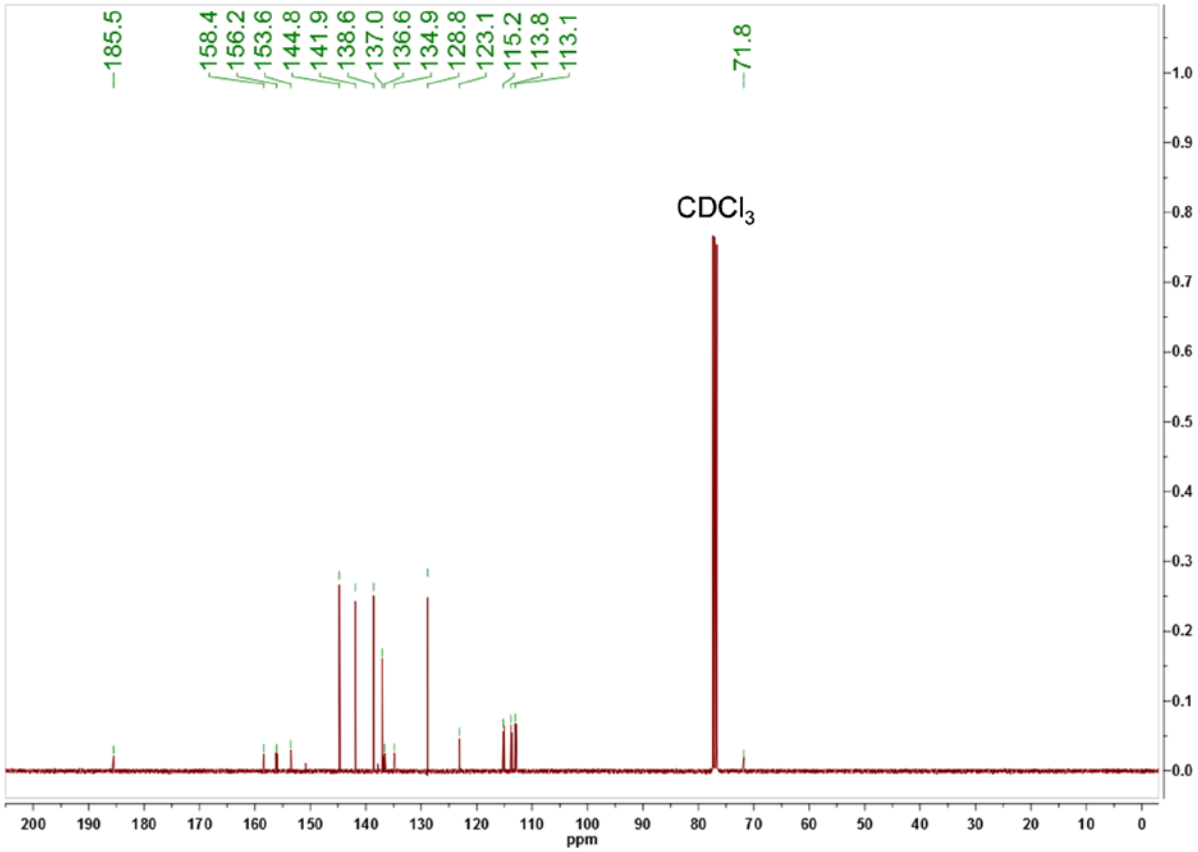

Fig. S24 ^{13}C NMR spectra of T-2F.

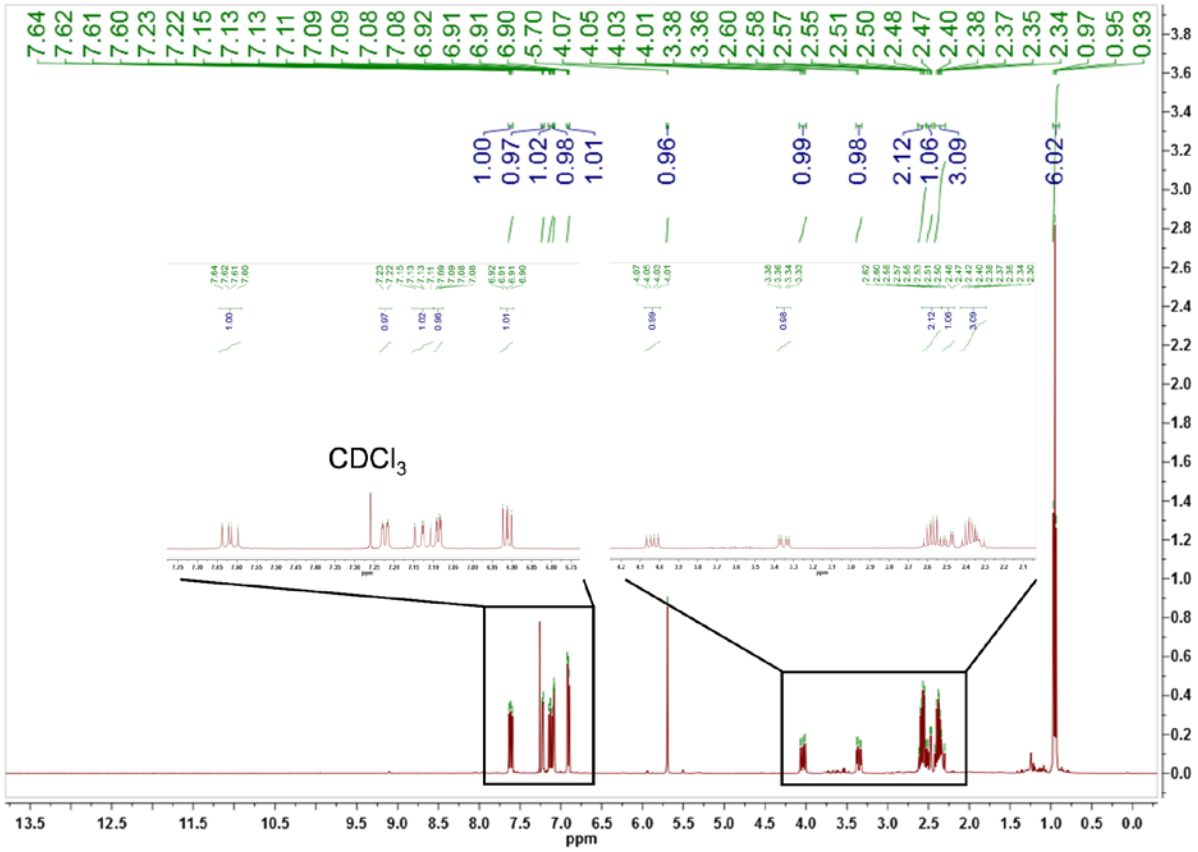

Fig. S25 ^{1}H NMR spectra of the product between T-2F and DEDA at RT.

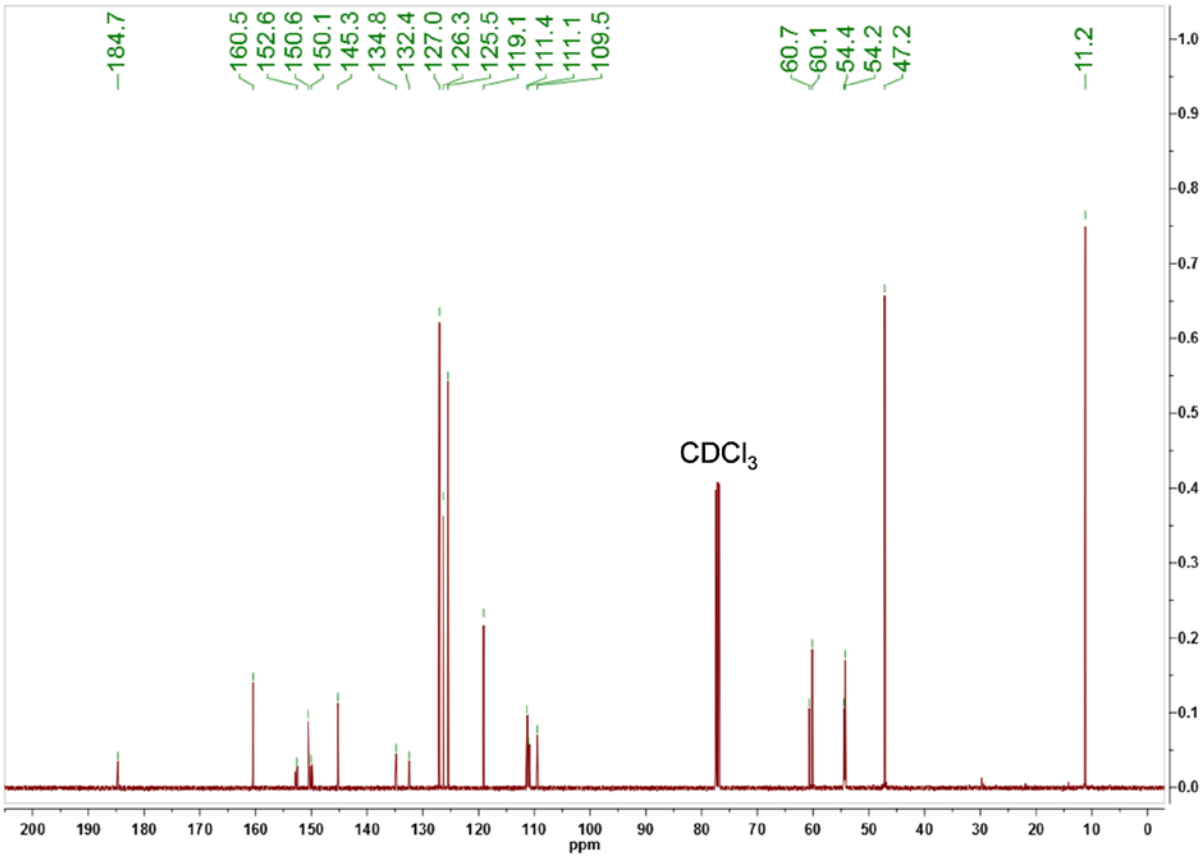

Fig. S26 ^{13}C NMR spectra of the product between T-2F and DEDA at RT.

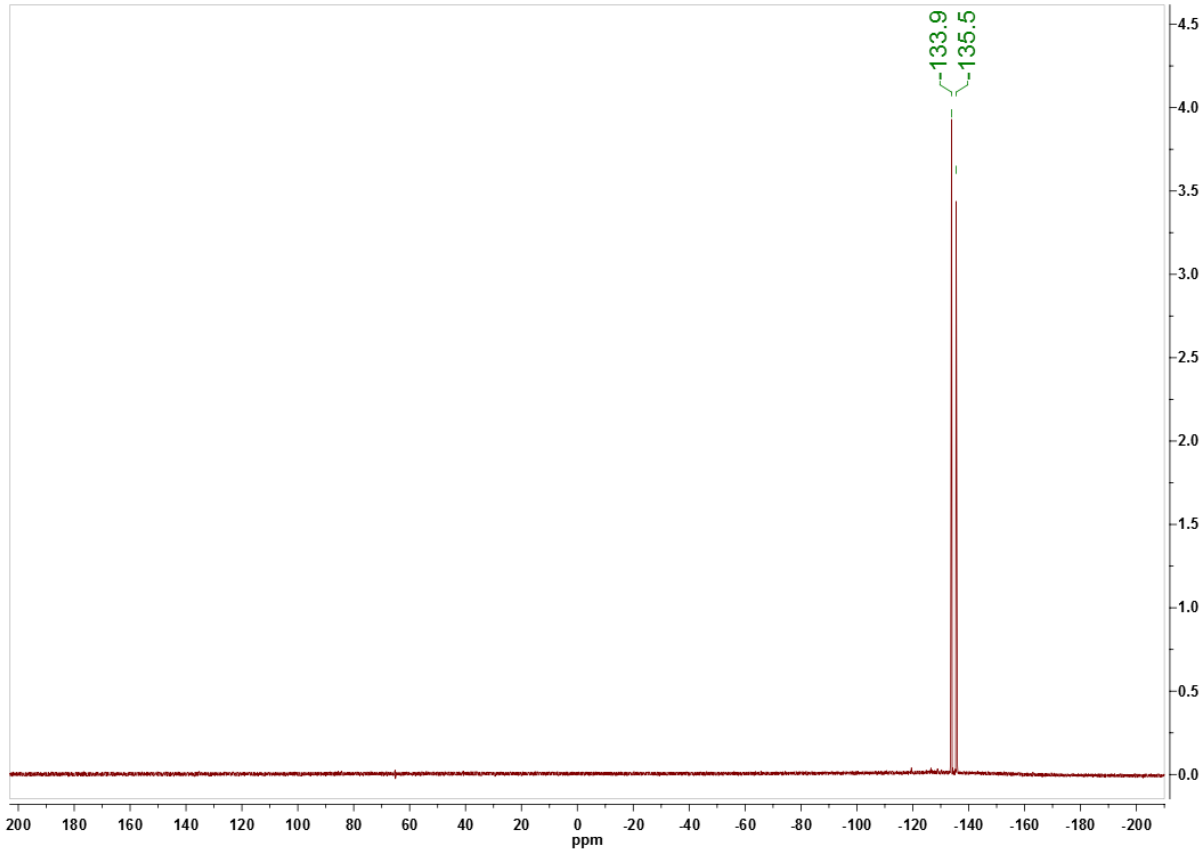

Fig. S27 ^{19}F NMR spectra of the product between T-2F and DEDA at RT.

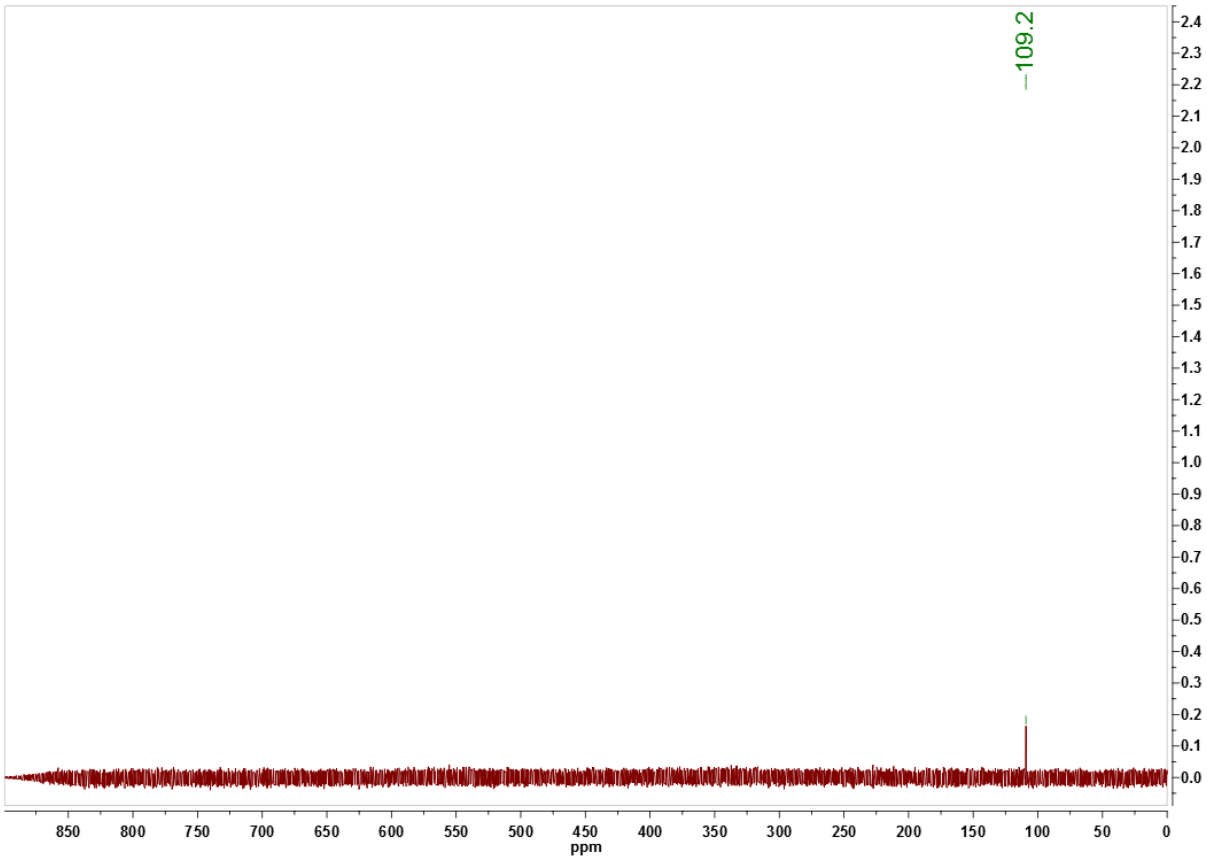

Fig. S28 ^{15}N NMR spectra of the product between T-2F and DEDA-^{15}N at RT.

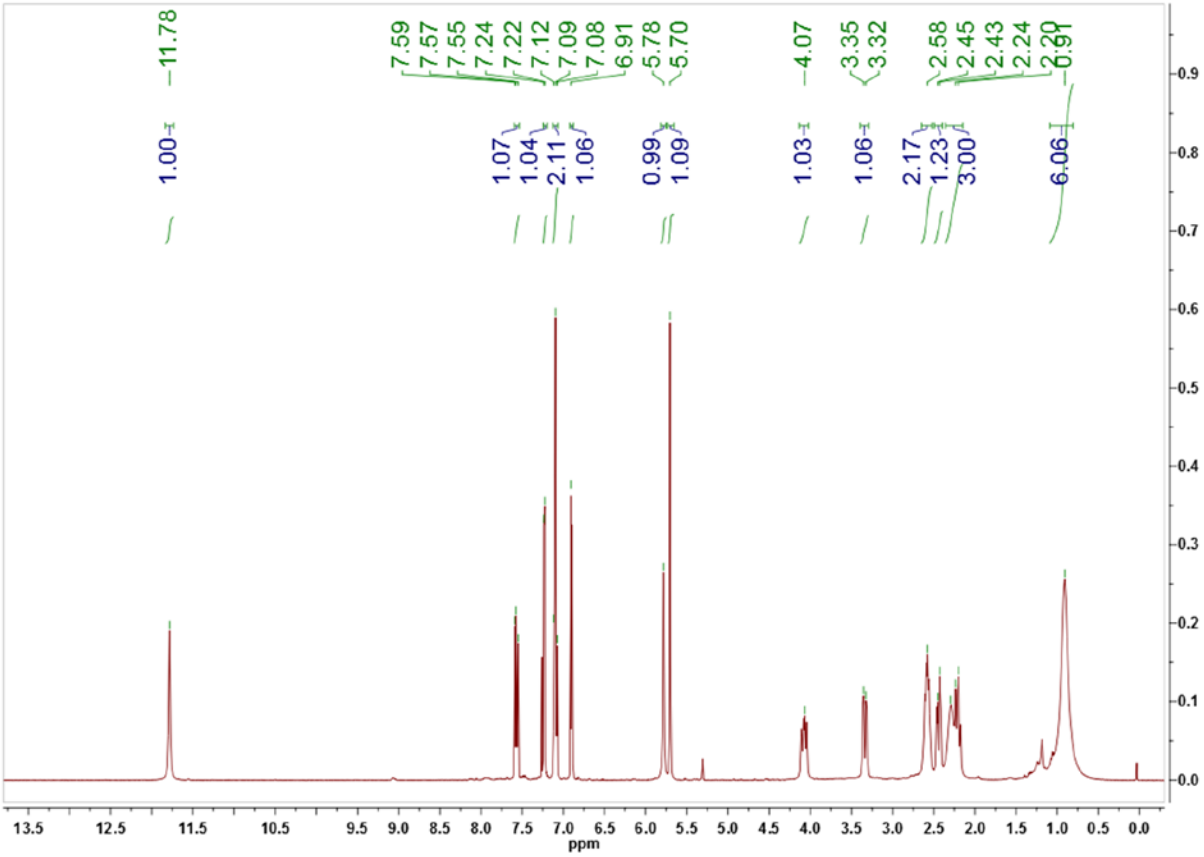

Fig. S29 ^{1}H NMR spectra of the product between T-2F and DEDA at -50°C.

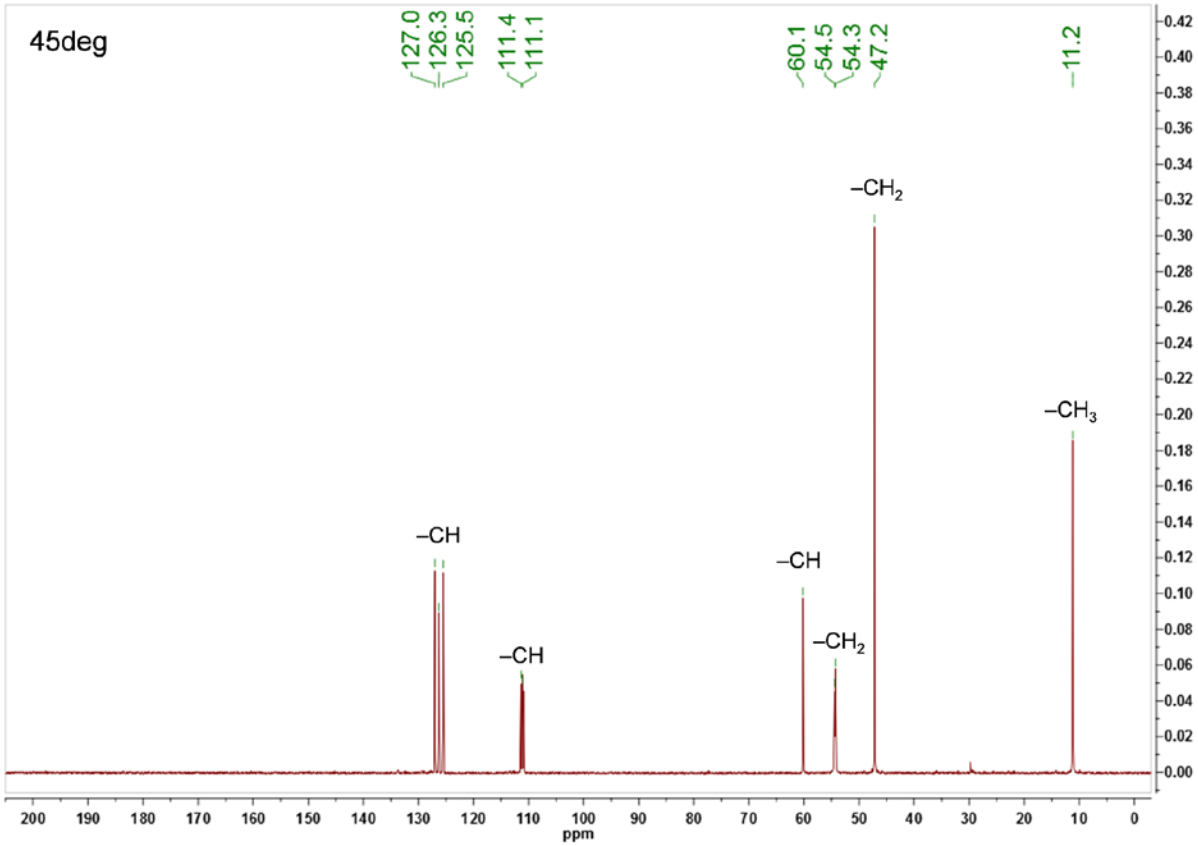

Fig. S30 ^{13}C/DEPT NMR spectra of the product between T-2F and DEDA at RT.

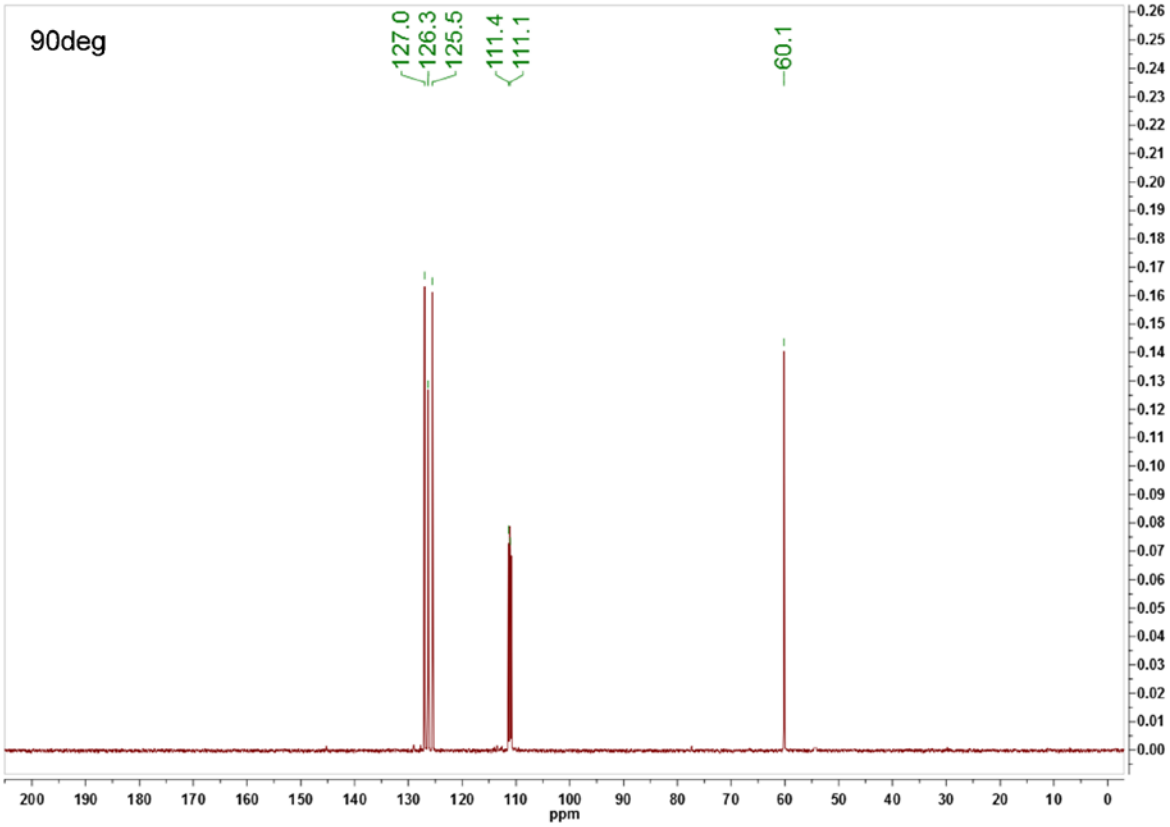

Fig. S31 ^{13}C/DEPT NMR spectra of the product between T-2F and DEDA at RT.

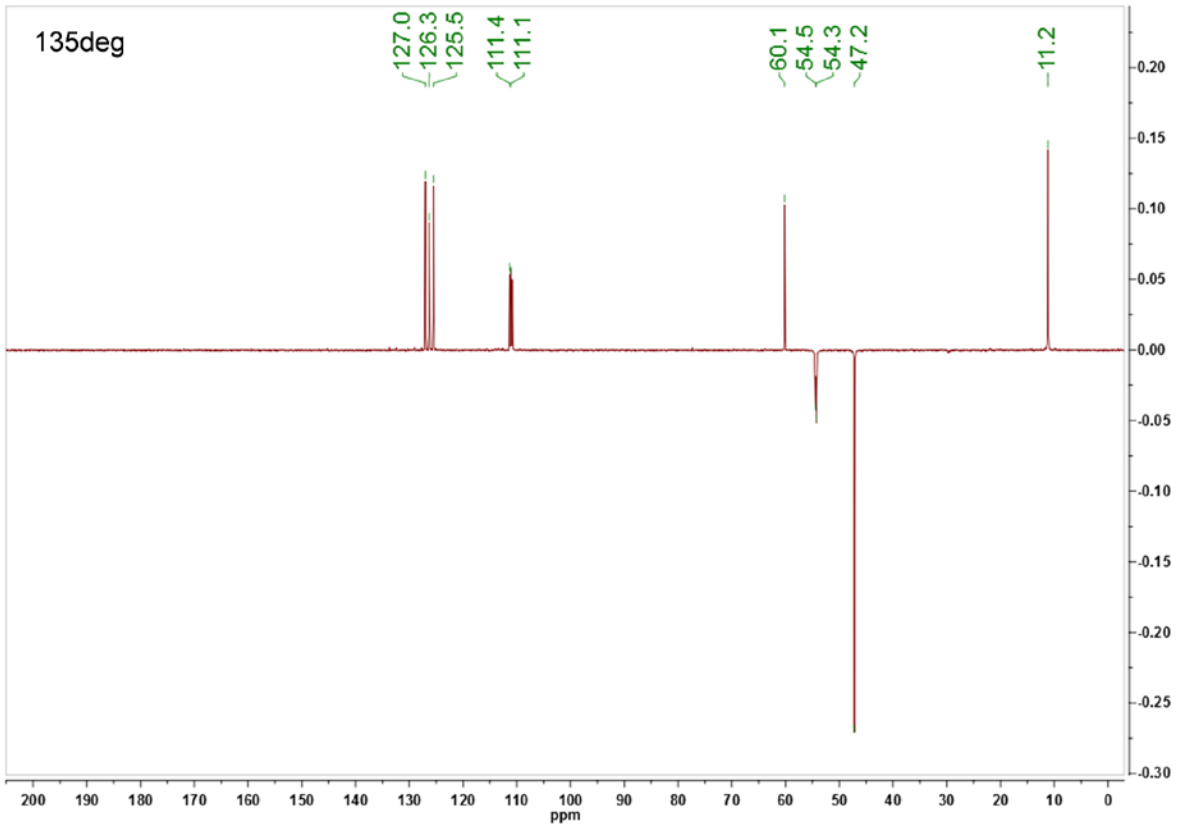

Fig. S32 ^{13}C/DEPT NMR spectra of the product between T-2F and DEDA at RT.

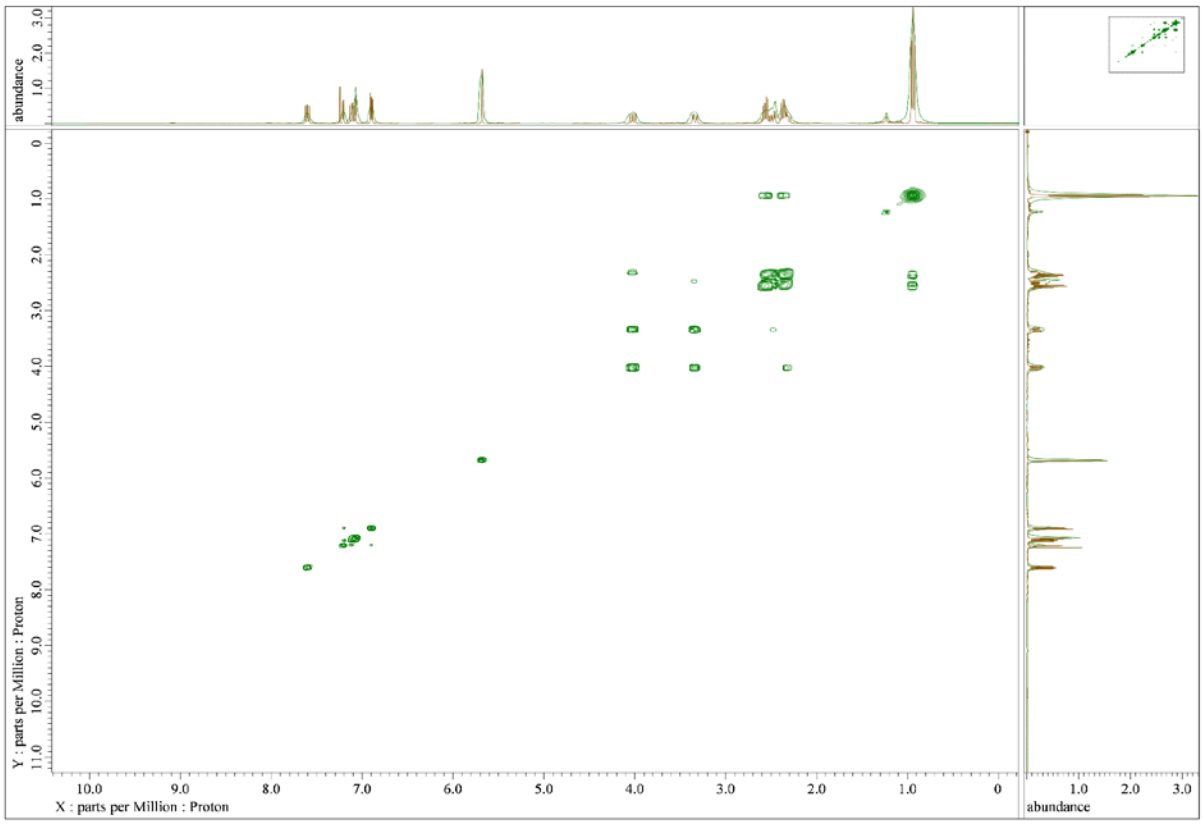

Fig. S33 COSY NMR spectra of the product between T-2F and DEDA at RT.

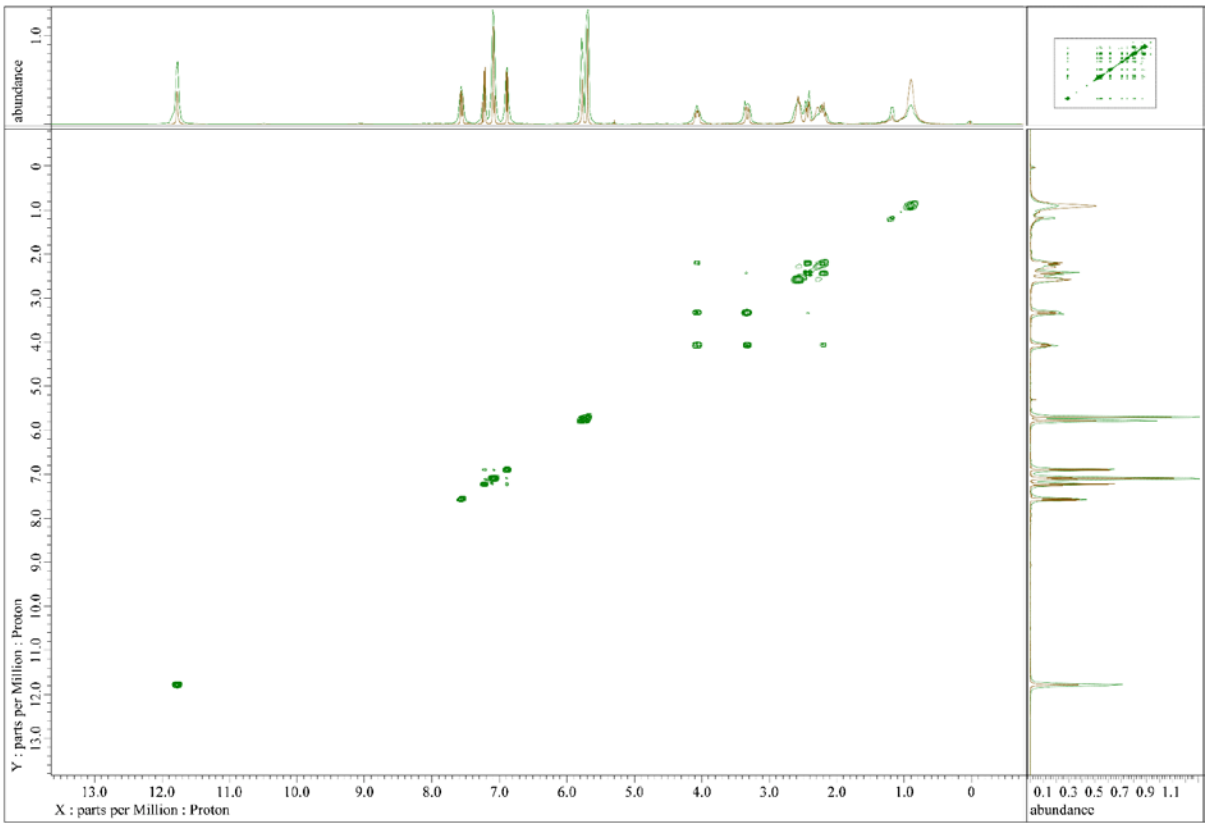

Fig. S34 COSY NMR spectra of the product between T-2F and DEDA at -50°C.

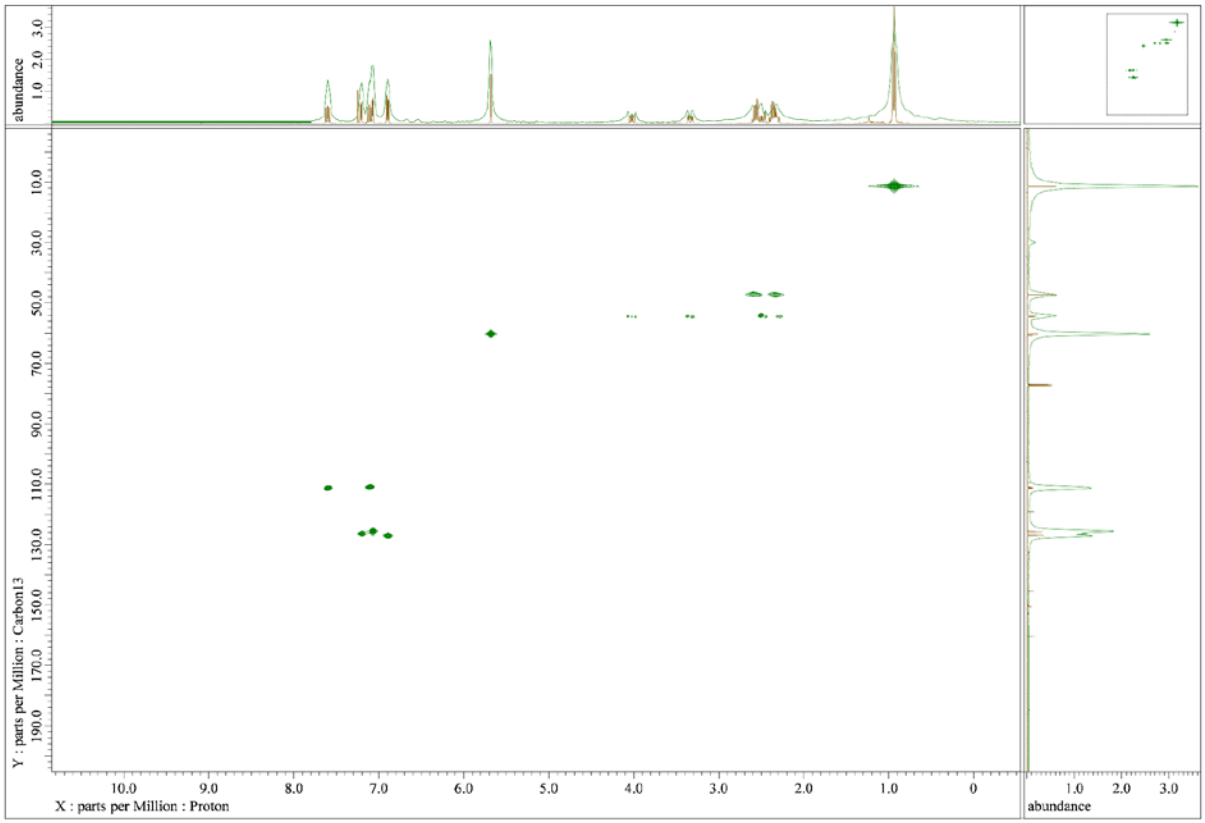

Fig. S35 ^{1}H–^{13}C HMQC NMR spectra of the product between T-2F and DEDA at RT.

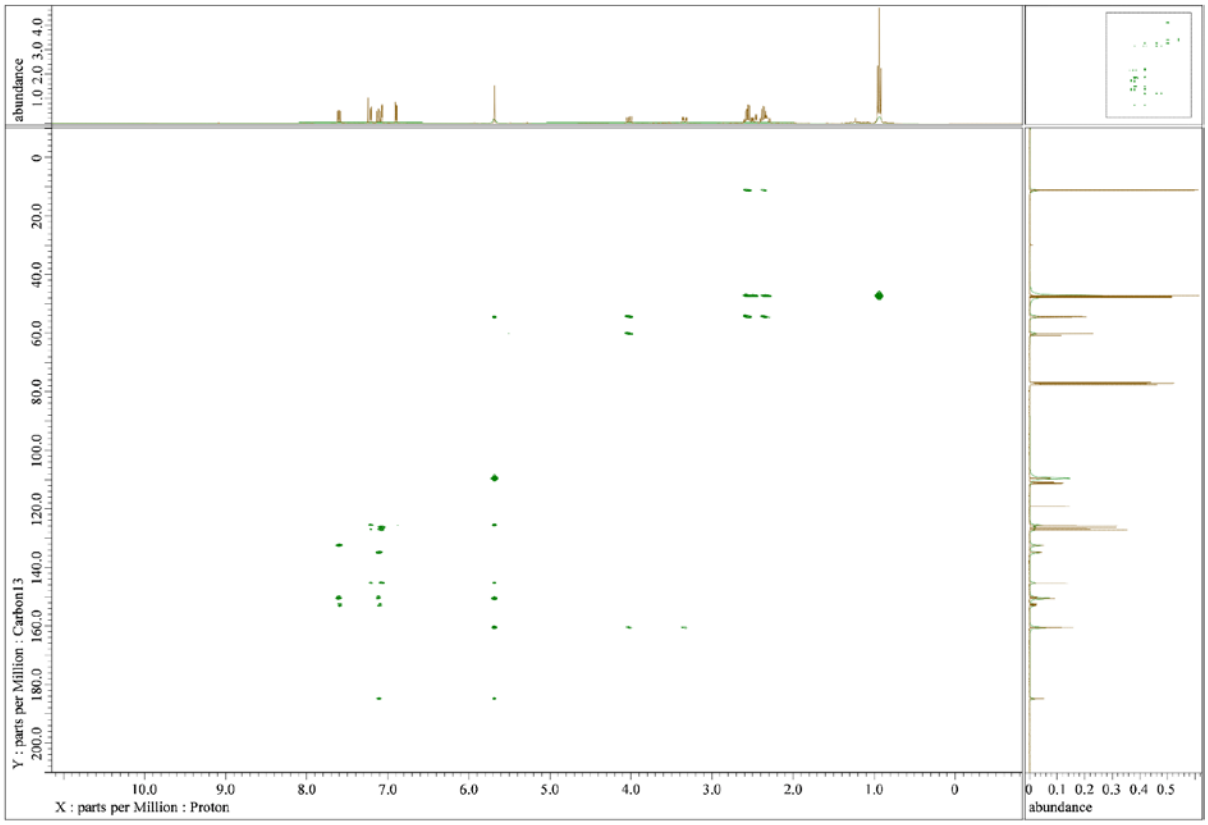

Fig. S36 $^{1}H–^{13}C$ HMBC NMR spectra of the product between T-2F and DEDA at RT.

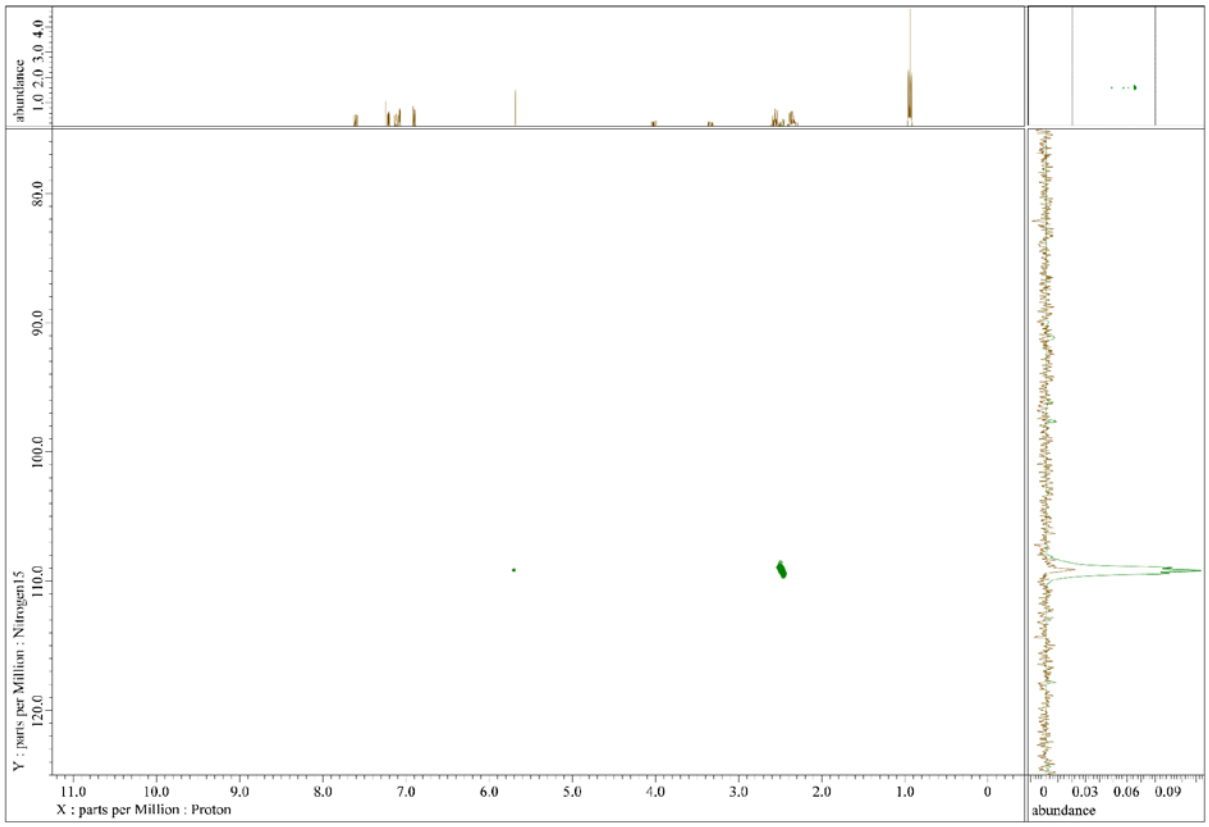

Fig. S37 $^{1}H–^{15}N$ HMBC NMR spectra of the product between T-2F and DEDA at RT.

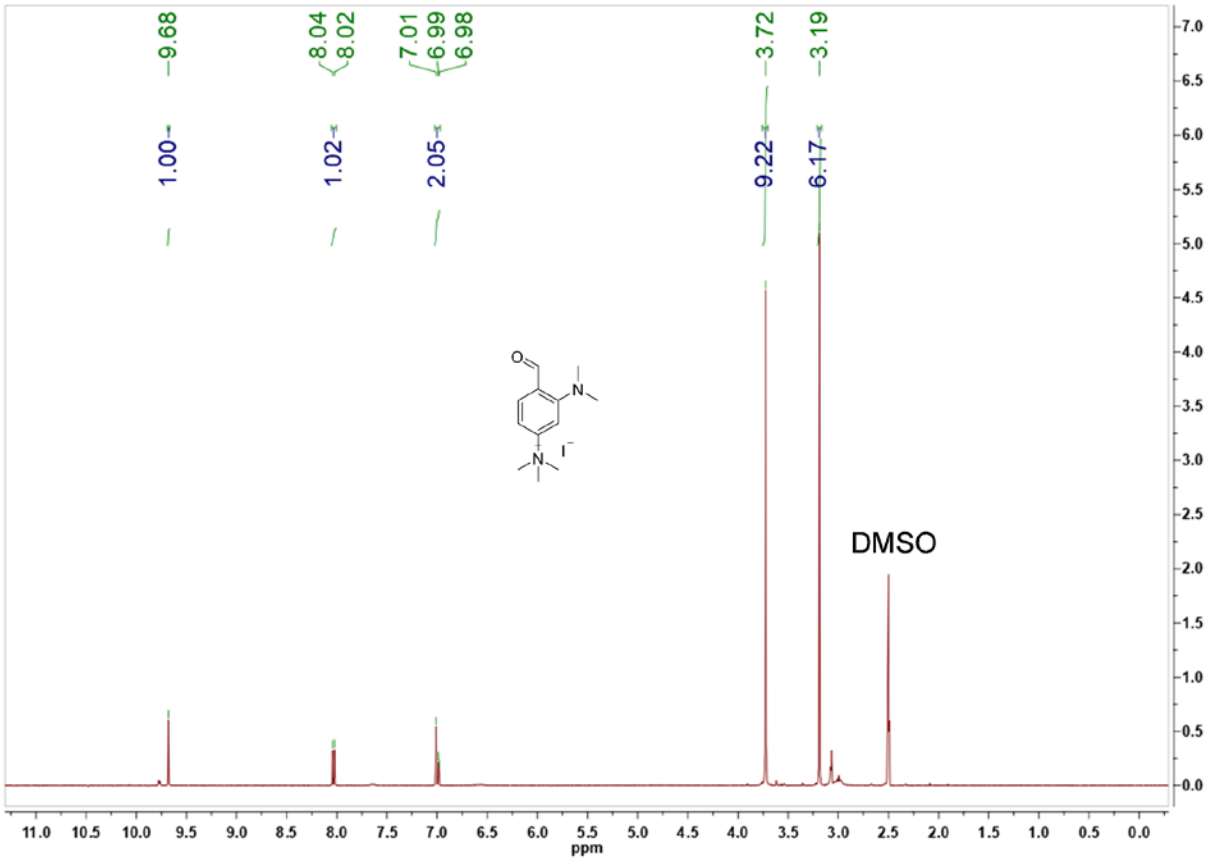

Fig. S38 ^{1}H NMR spectra of 3.

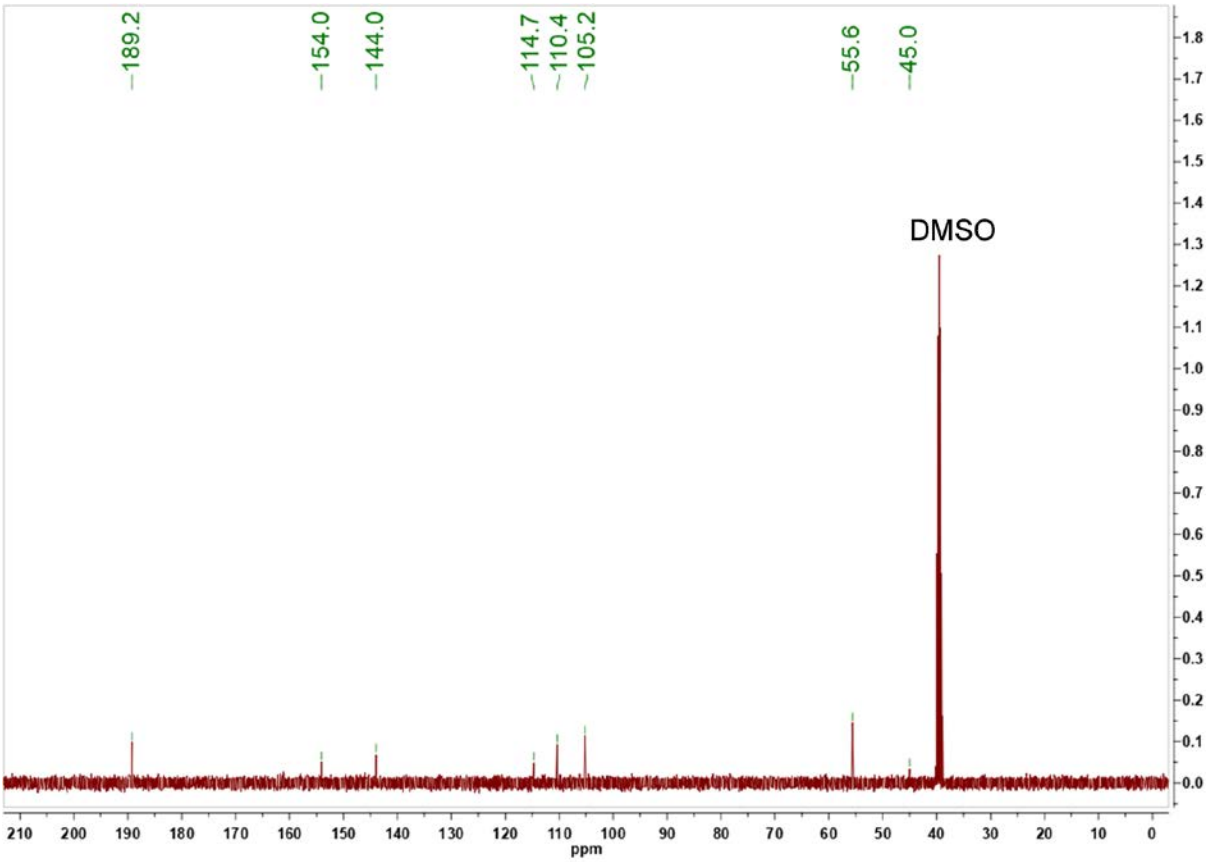

Fig. S39 ^{13}C NMR spectra of 3.

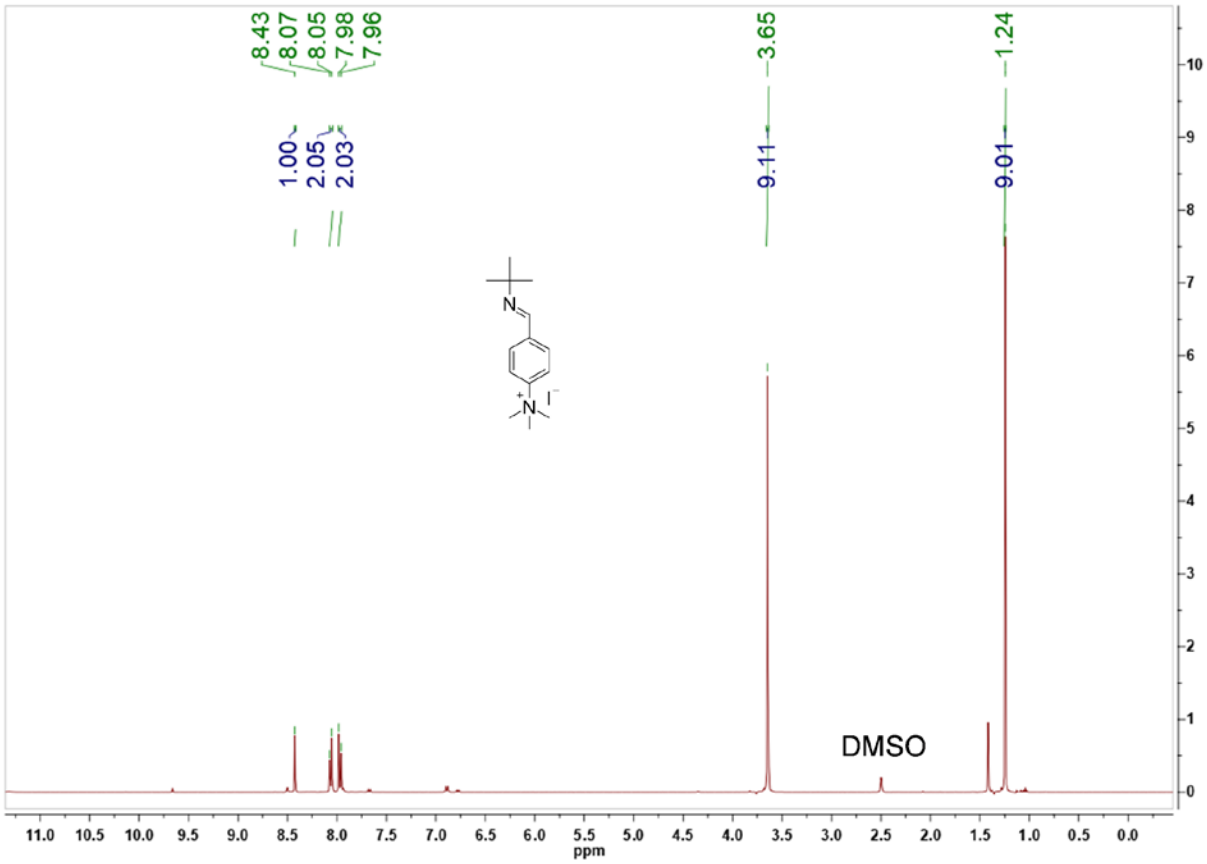

Fig. S40 ^{1}H NMR spectra of tBu-N.

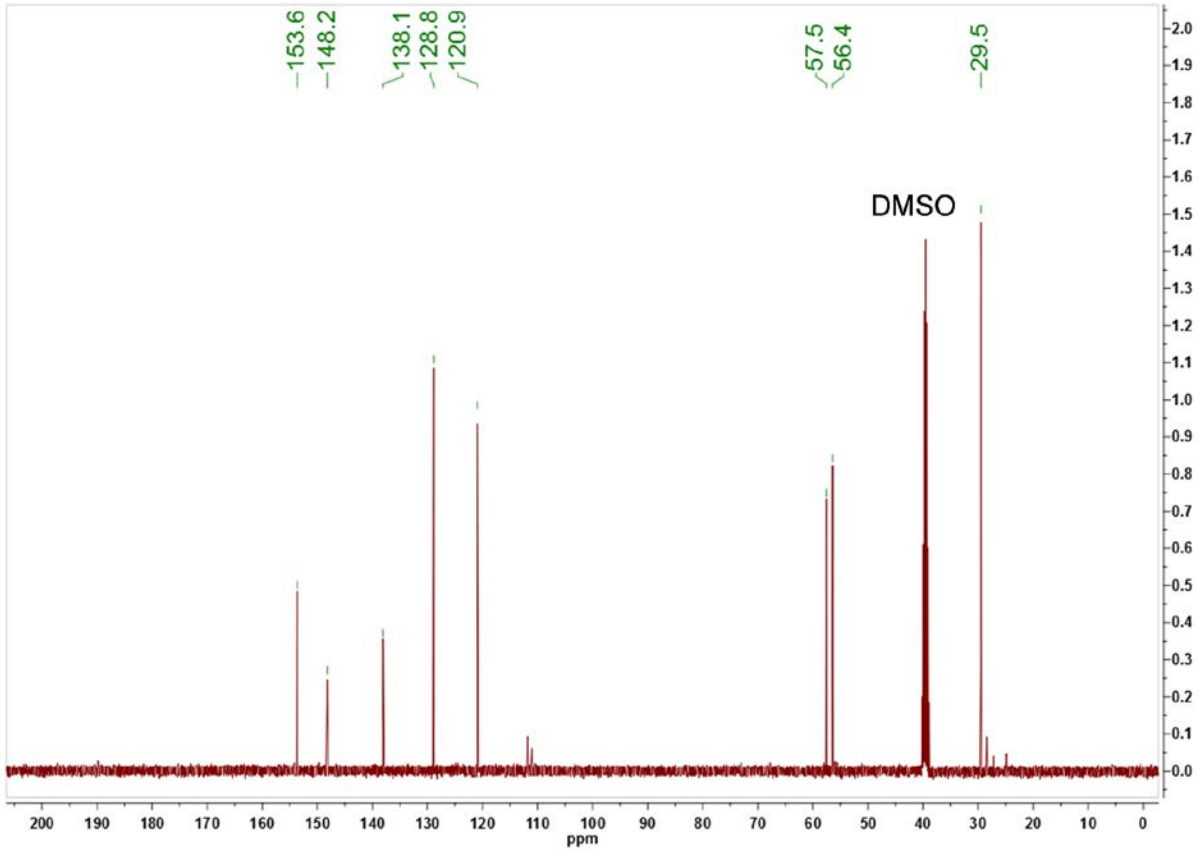

Fig. S41 ^{13}C NMR spectra of tBu-N.

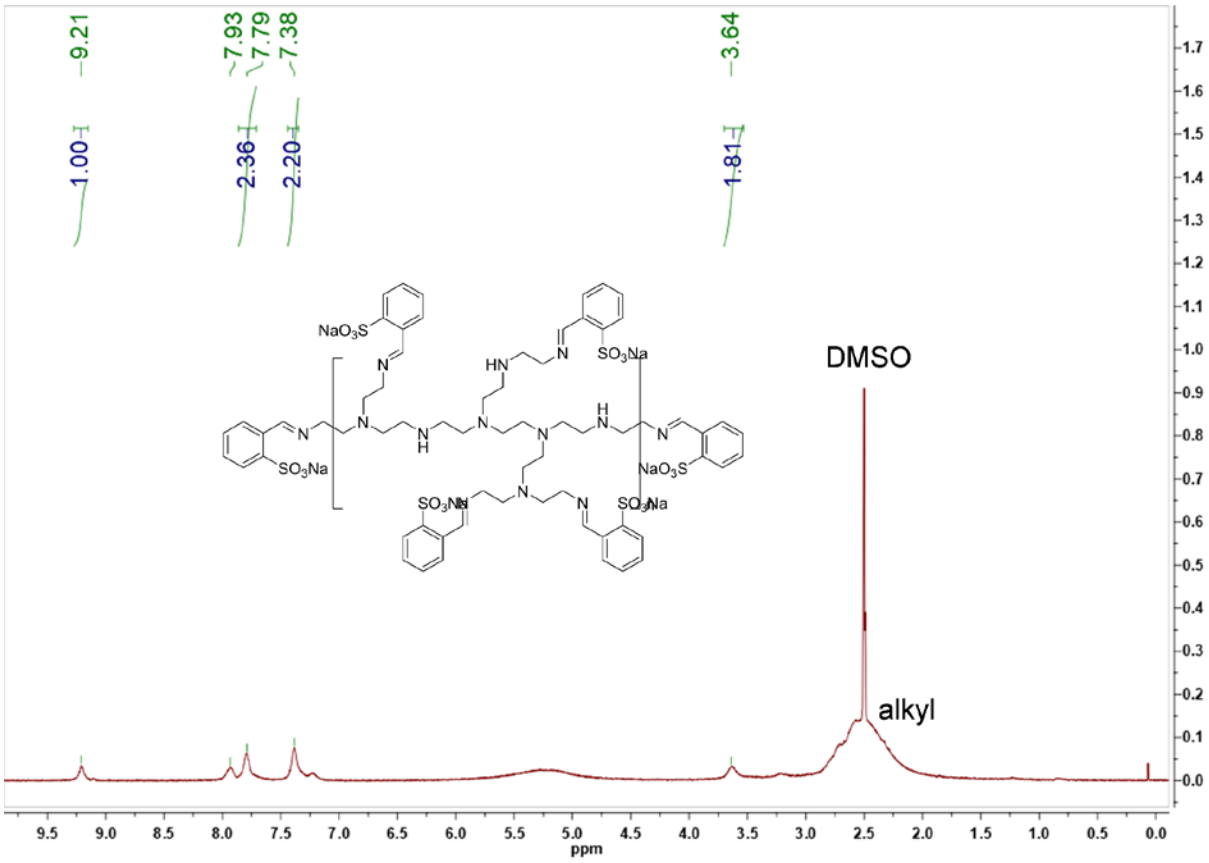

Fig. S42 ^{1}H NMR spectra of PEI-S.

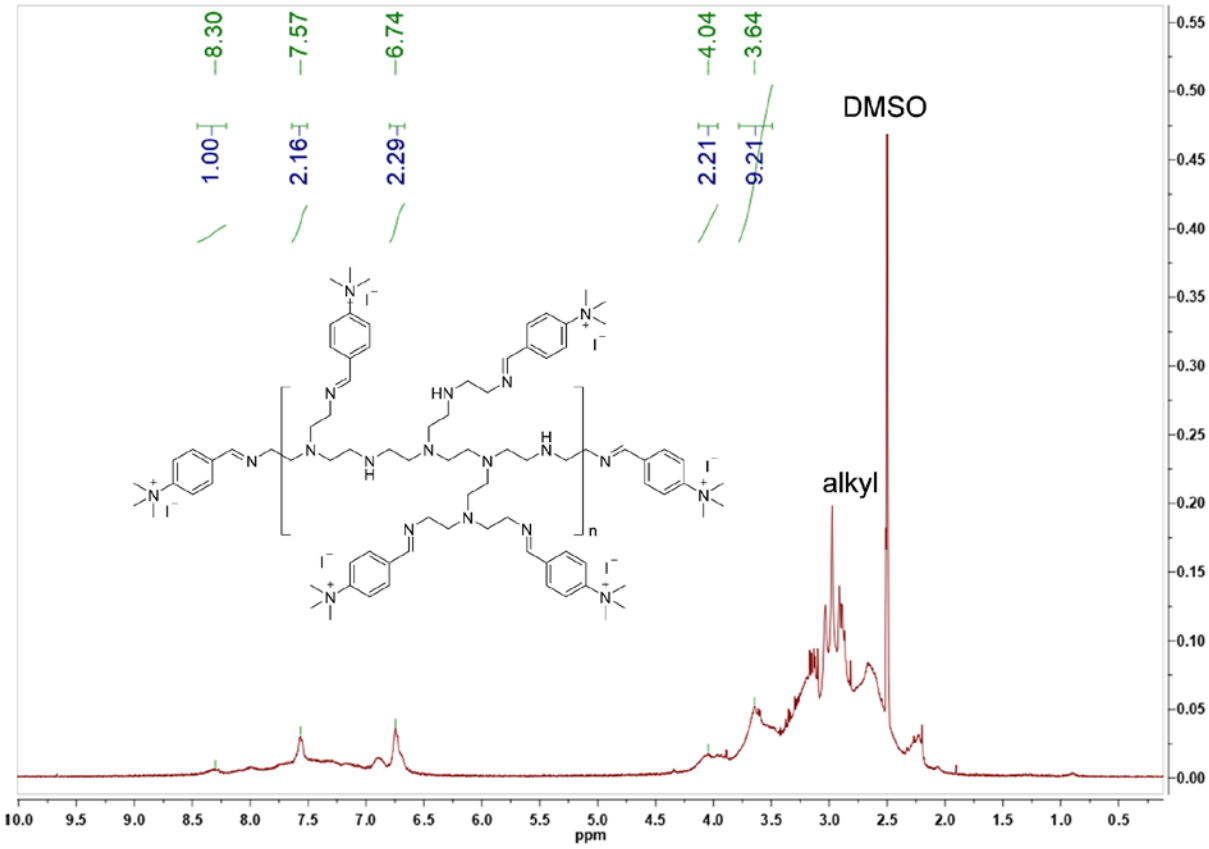

Fig. S43 ^{1}H NMR spectra of PEI-N.

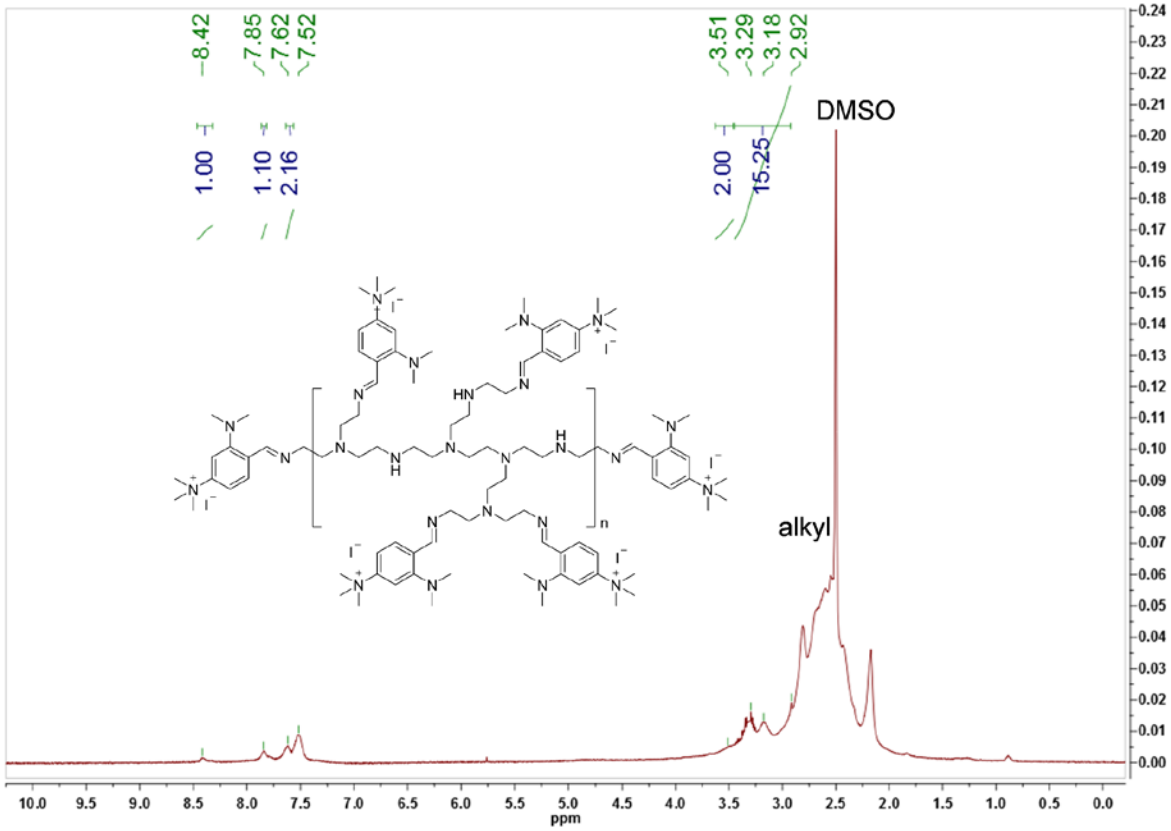

Fig. S44 ^{1}H NMR spectra of PEI-NdMeN.

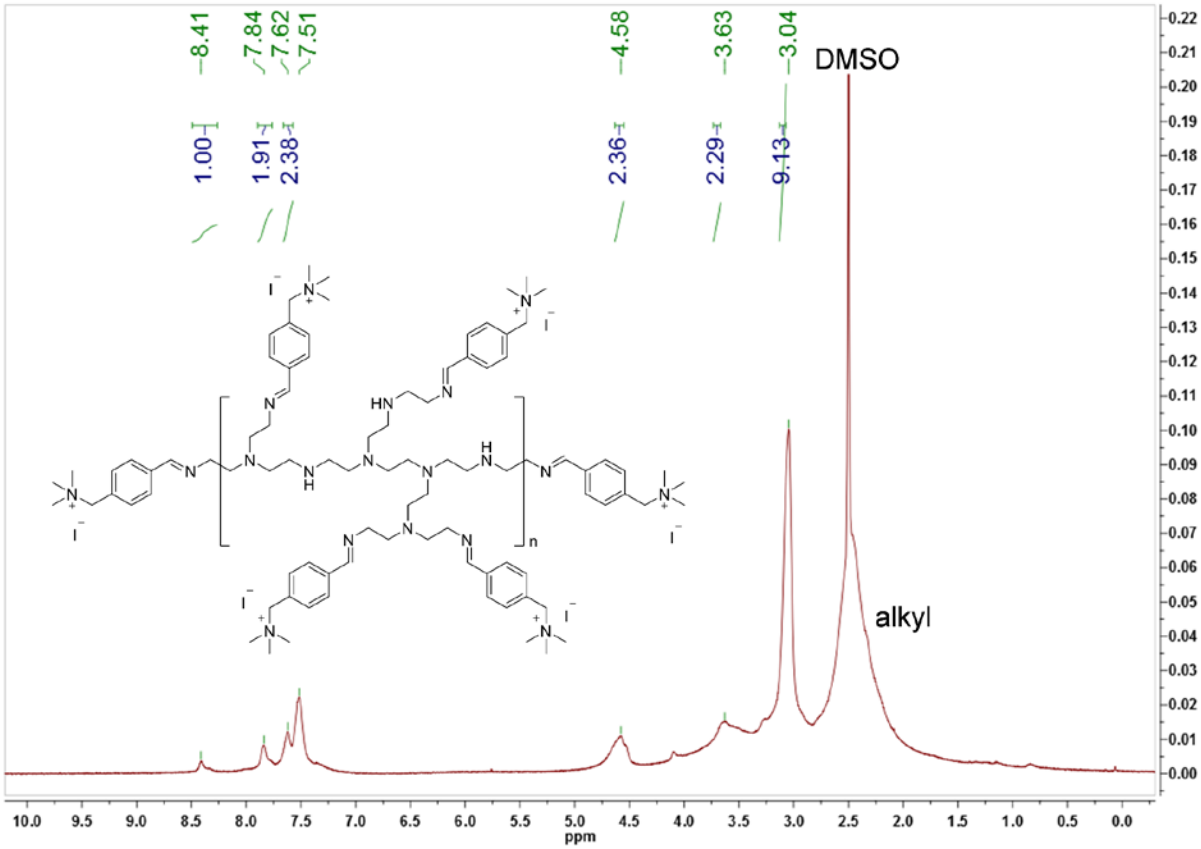

Fig. S45 ^{1}H NMR spectra of PEI-mNI.

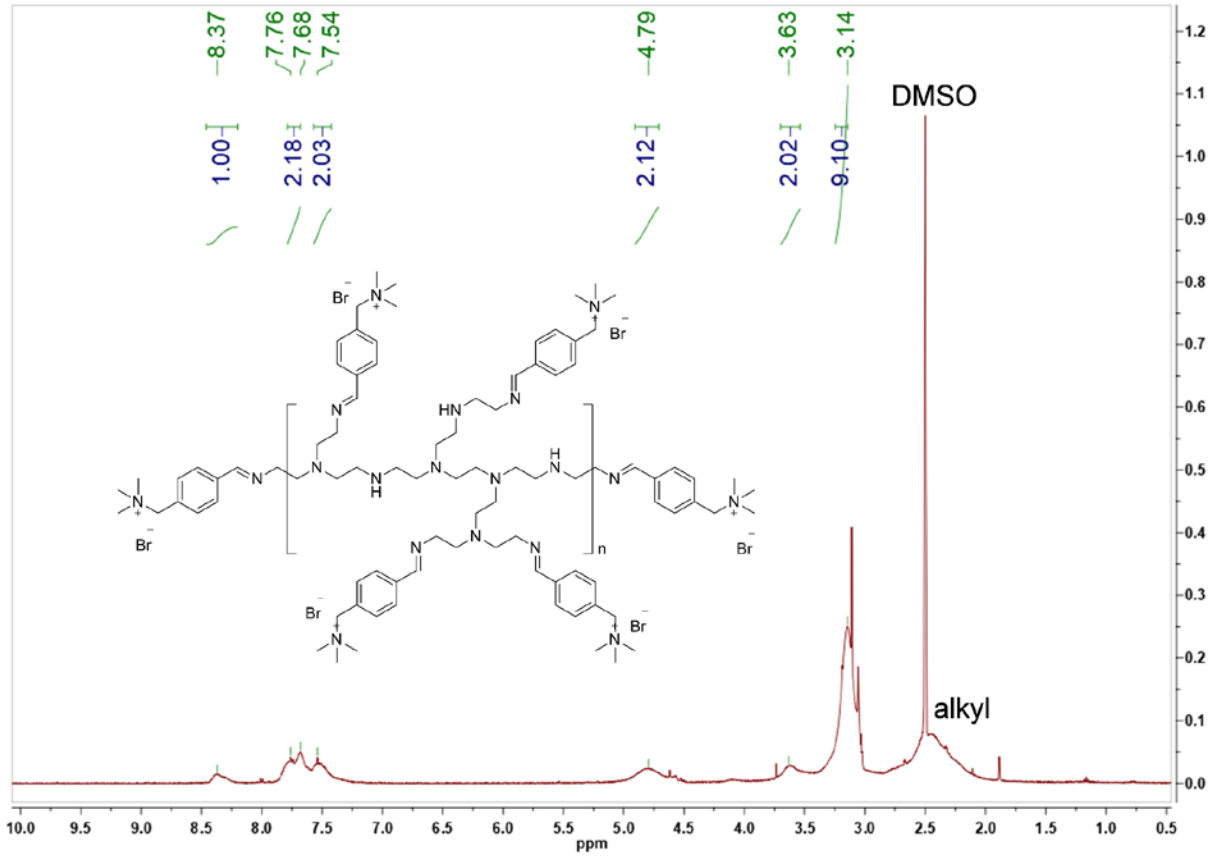

Fig. S46 ^{1}H NMR spectra of PEI-mNBr.

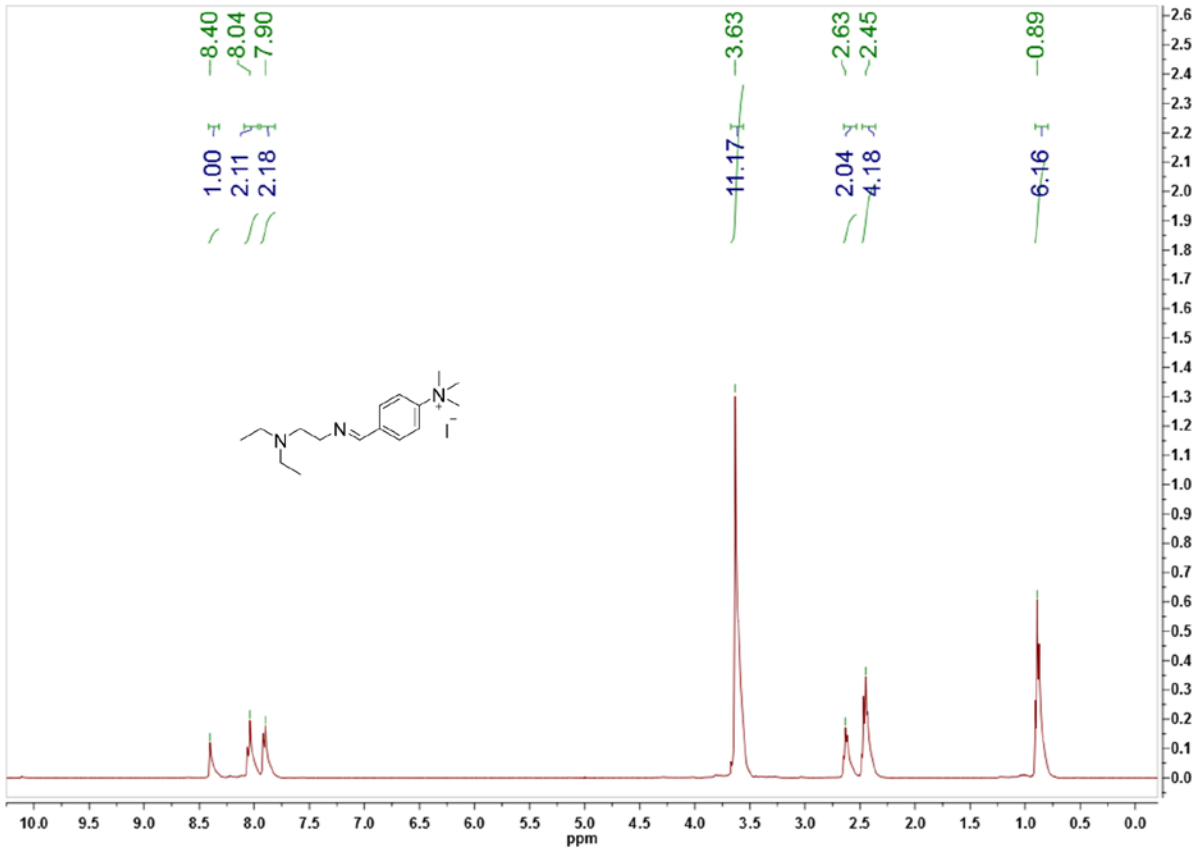

Fig. S47 ^{1}H NMR spectra of TEA-N.

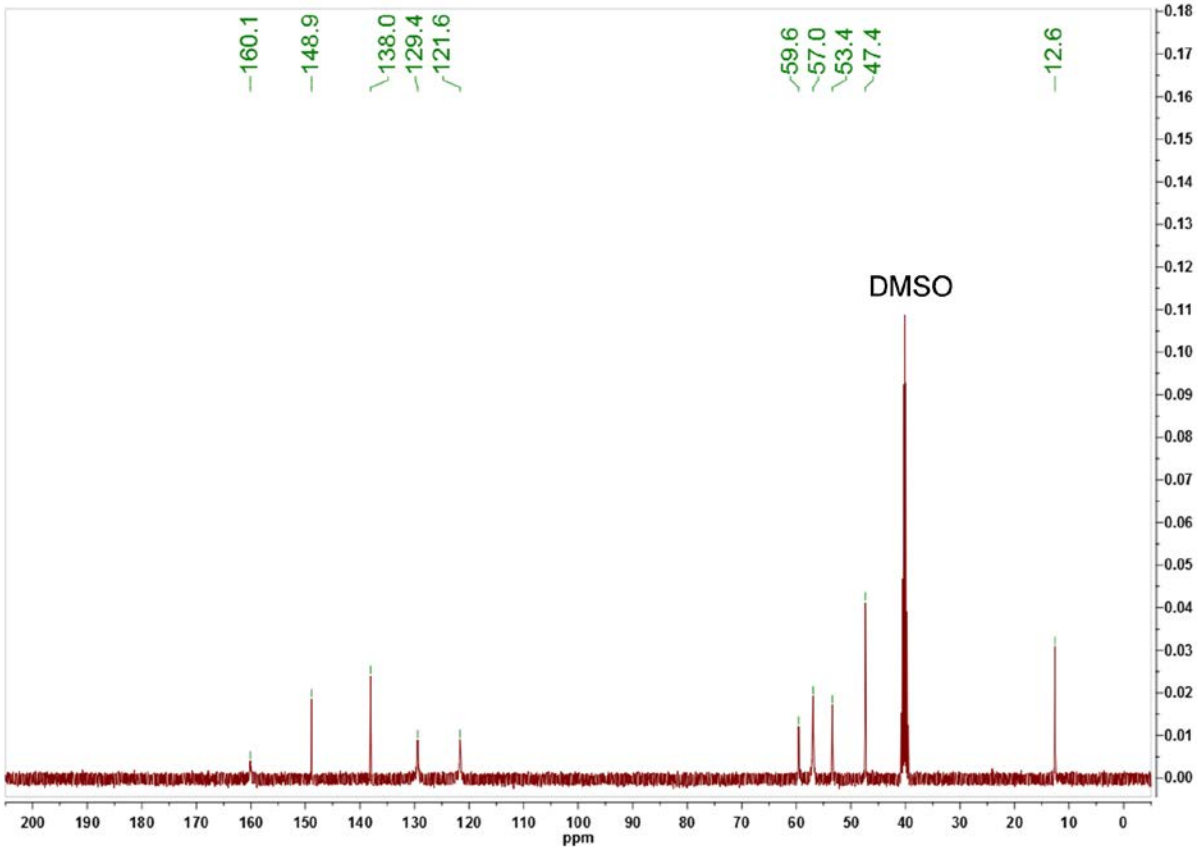

Fig. S48 ^{13}C NMR spectra of TEA-N.

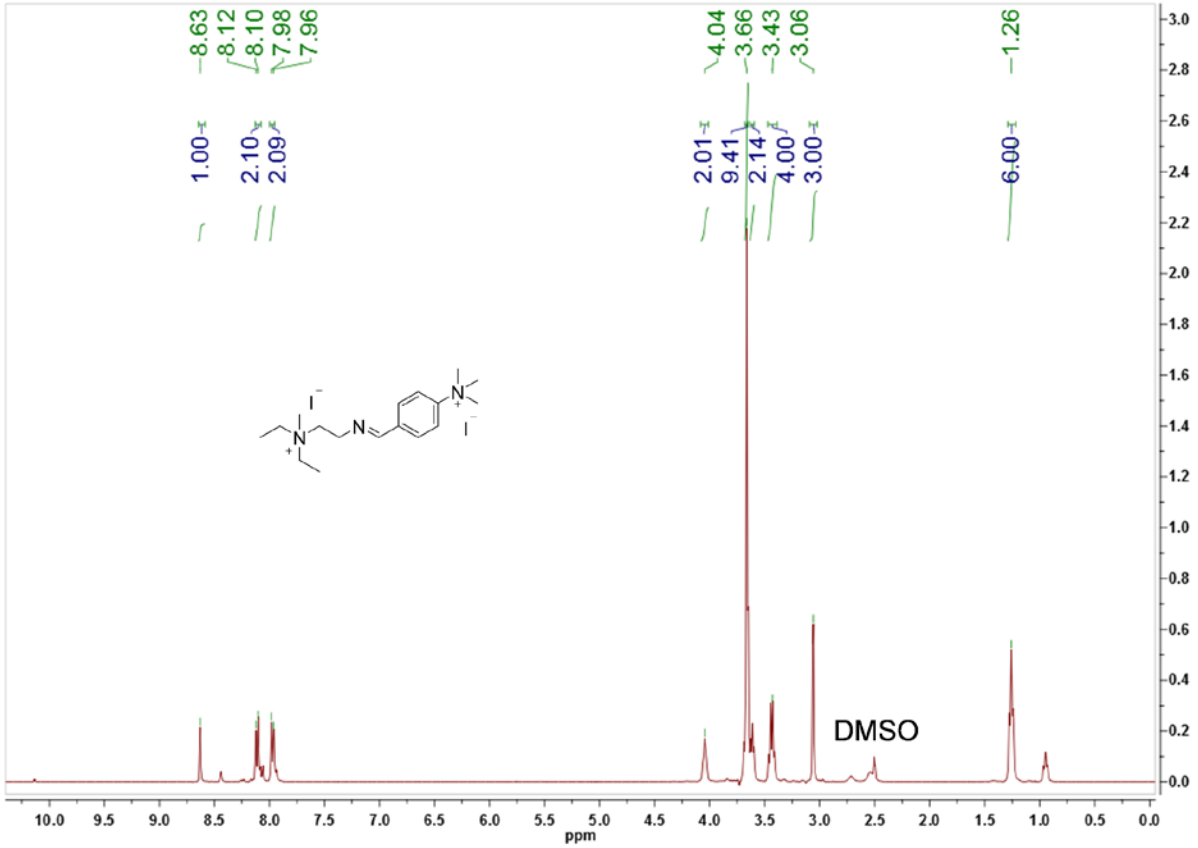

Fig. S49 ^{1}H NMR spectra of MeTEA-N.

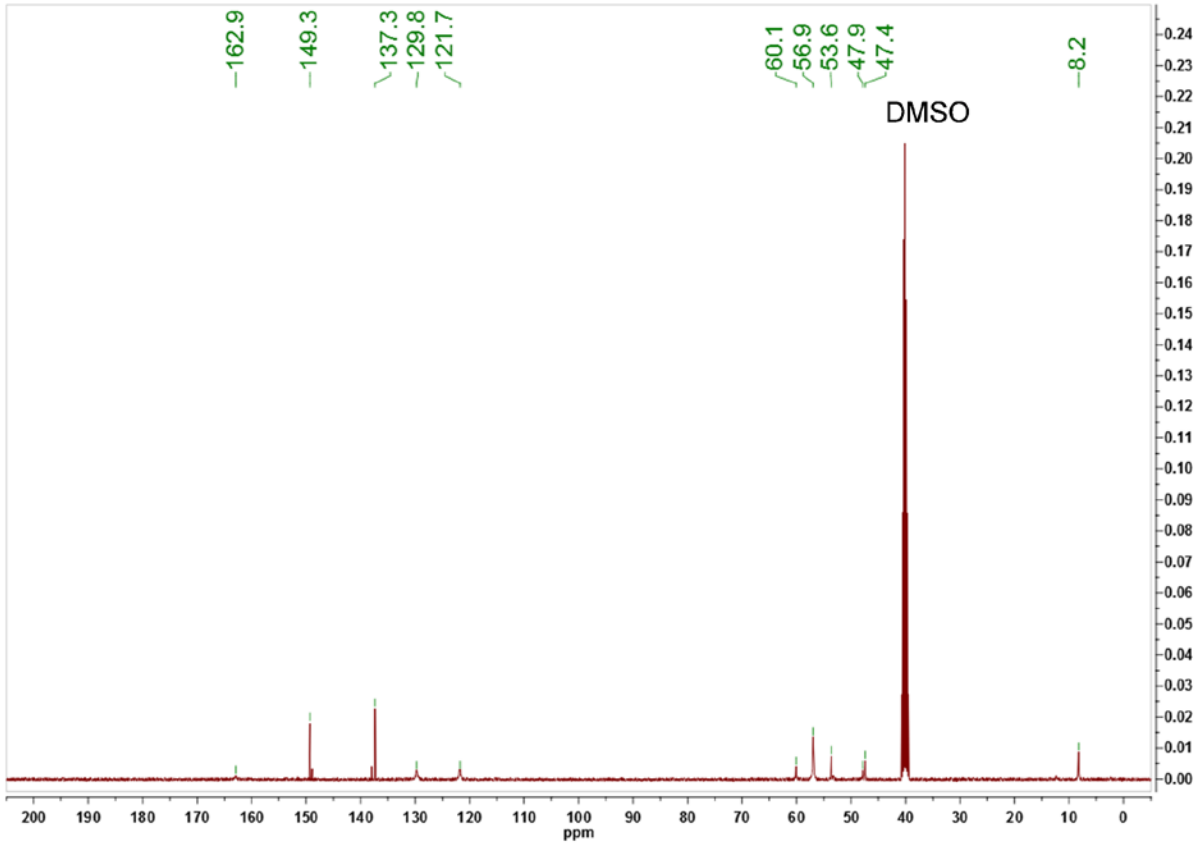

Fig. S50 ^{13}C NMR spectra of MeTEA-N.

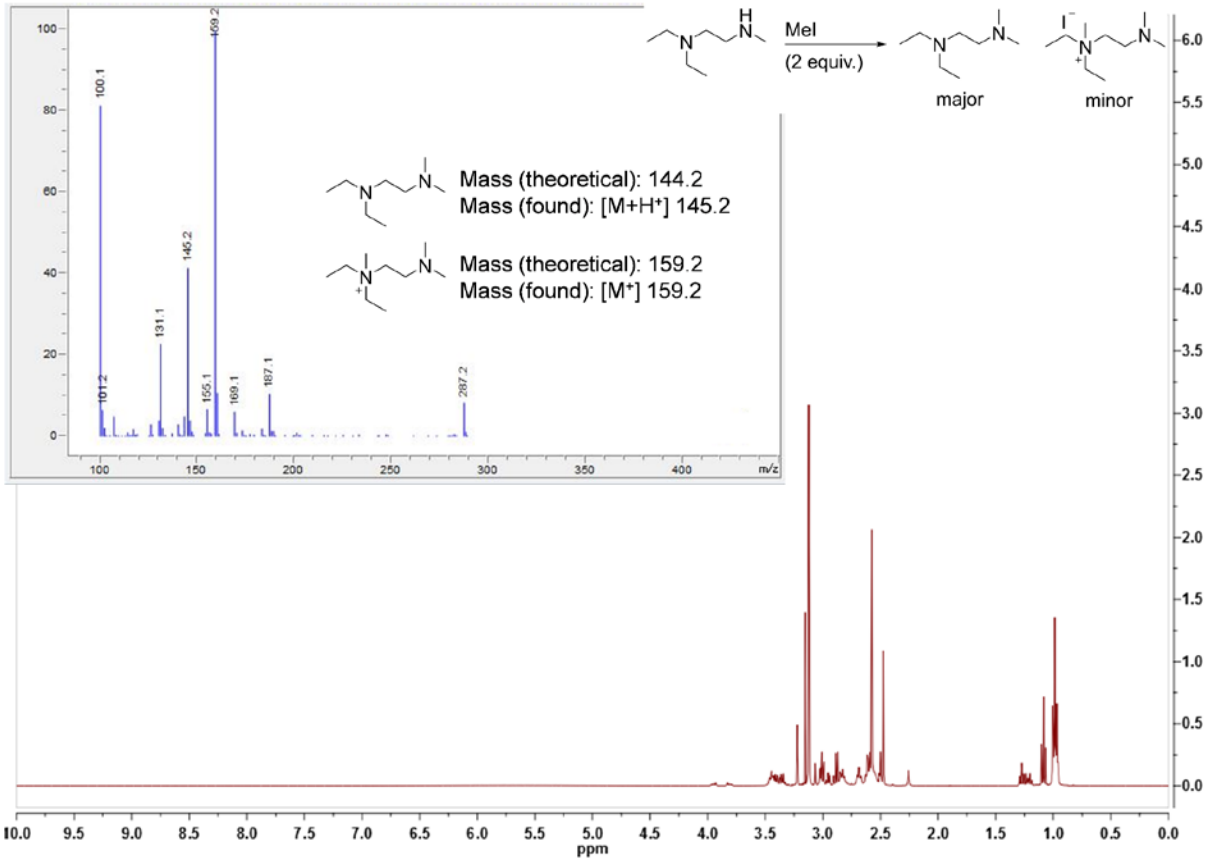

Fig. S51 ^{1}H NMR spectra and LC-MS data of the crude product which was produced from *N*,*N*-Diethyl-*N*'-methylethylenediamine and 2 equivalents of MeI.

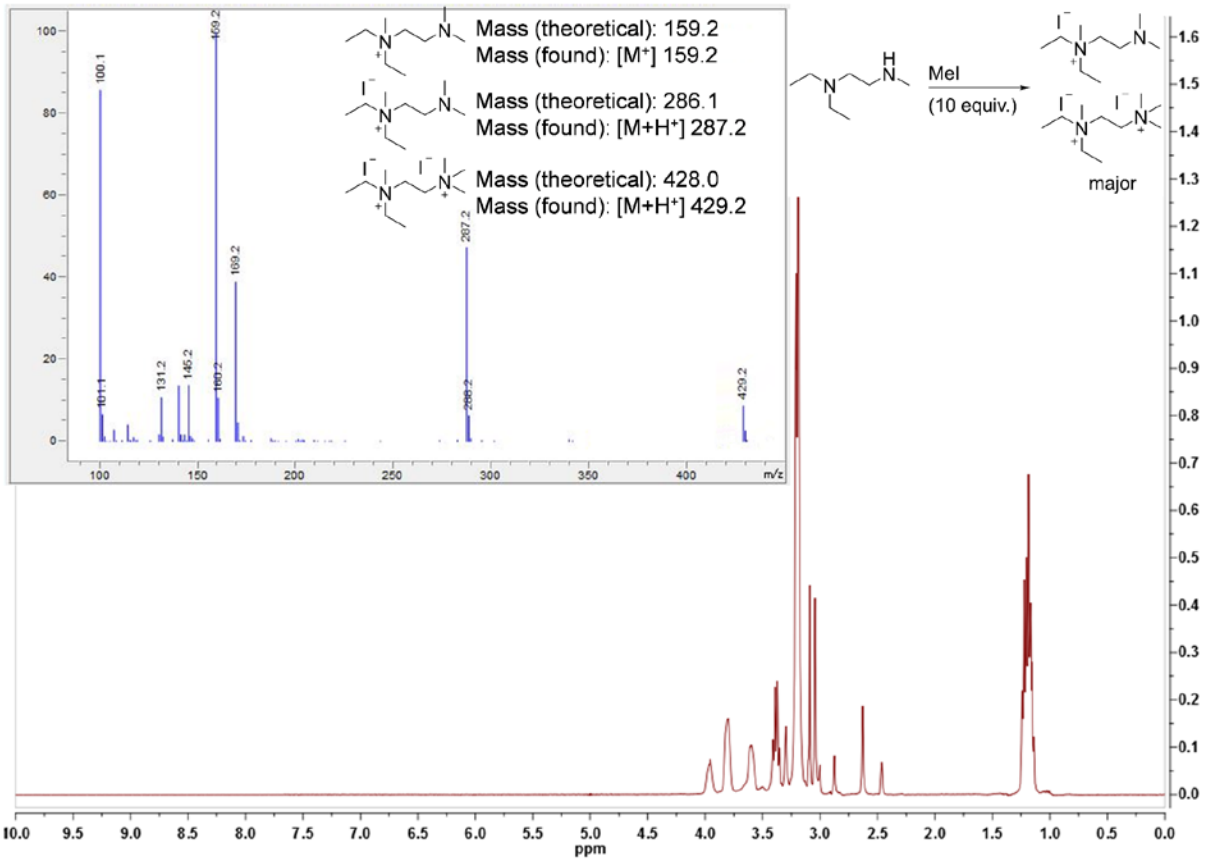

Fig. S52 ^{1}H NMR spectra and LC-MS data of the crude product which was produced from *N*,*N*-Diethyl-*N*'-methylethylenediamine and 10 equivalents of MeI.

8. References

1 H. Yao, Y. Cui, R. Yu, B. Gao, H. Zhang, J. Hou, *Angew. Chem. Int. Ed.* 2017, **56**, 3045-3049.

2 H. Yuan, Z. Zhou, J. Xiao, L. Liang, L. Dai, *Tetrahedron: Asymmetry*. 2010, **21**, 1874-1884.

3 J. Garcia, J. Sorrentino, E. J. Diller, D. Chapman, Z. R. Woydziak, *Synth. Commun.* 2016, **46**, 475-481.

4 J. A. Sindac, S. J. Barraza, C. J. Dobry, J. Xiang, P. K. Blakely, D. N. Irani, R. F. Keep, D. J. Miller, S. D. Larsen, *J. Med. Chem.* 2013, **56**, 9222-9241.

5 C. B. Minkenberg, L. Florusse, R. Eelkema, G. J. Koper, J. H. van Esch, *J. Am. Chem. Soc.* 2009, **131**, 11274-11275.

6 M. Kyeong, J. Lee, K. Lee, S. Hong, *ACS. Appl. Mater. Interfaces.* 2018, **10**, 23254-23262.

7 M. Iwata, H. Kuzuhara, *Chemistry Letters.* 1986, **15**, 369-372.

8 H. Tazarki, W. Zeinyeh, Y. J. Esvan, S. Knapp, D. Chatterjee, M. Schroder, A. C. Joerger, J. Khiari, B. Josselin, B. Baratte, S. Bach, S. Ruchaud, F. Anizon, F. Giraud, P. Moreau, *Eur. J. Med. Chem.* 2019, **166**, 304-317.

9 V. D. Mihailetchi, H. X. Xie, B. de Boer, L. J. A. Koster, P. W. M. Blom, *Adv. Funct. Mater.* 2006, **16**, 699-708.

10 X. Song, N. Gasparini, M. M. Nahid, H. Chen, S. M. Macphee, W. M. Zhang, V. Norman, C. H. Zhu, D. Bryant, H. Ade, I. McCulloch, D. Baran, *Adv. Funct. Mater.* 2018, **28**, 1802895.